https://doi.org/10.15407/ufm.25.03.482

V.G. GAVRILJUK*, V.M. SHYVANIUK, and S.M. TEUS*****
G.V. Kurdyumov Institute for Metal Physics of the N.A.S. of Ukraine,
36 Academician Vernadsky Blvd., UA-03142 Kyiv, Ukraine

* gavr@imp.kiev.ua, ** shyva@imp.kiev.ua, *** teus@imp.kiev.ua

ELECTRON CONCEPT OF HYDROGEN EMBRITTLEMENT AND HYDROGEN-INCREASED PLASTICITY OF METALS

Based on theoretical and experimental studies of hydrogen effect on the electron structure of iron, nickel and titanium, an electron concept is proposed for hydrogen embrittlement as well as for hydrogen-improved plasticity of engineering metallic materials. This concept implies a hydrogen-caused redistribution of valence electrons across their energy levels and an increase in the density of electron states at the Fermi level, causing a softening of the crystal lattice and, thereby, leading to a decrease in the specific energy of dislocations with consequent increase in their mobility. Innate phenomena in metallic solid solutions, namely, short-range atomic order in its two versions, short-range ordering and decomposition, are shown to be a precondition for the localization of plastic deformation. Hydrogen enhances merely this effect resulting in pseudo-brittle fracture. The role of hydrogen-induced superabundant vacancies in hydrogen-caused localization of plastic deformation and grain-boundary fracture in pure metals is discussed. Using the temperature- and strain-dependent internal friction, the enthalpies of hydrogen diffusion and hydrogen–dislocation binding are studied, and their controlling effect on the temperature- and strain-rate-dependent hydrogen embrittlement is demonstrated. Finally, a physical rationale is proposed for using hydrogen as a temporary alloying element in the technological processing of titanium alloys, and for a positive hydrogen effect on the fatigue life and plasticity of austenitic steels.

Keywords: hydrogen, iron, nickel, titanium, electron structure, embrittlement, plasticity.

Citation: V.G. Gavriljuk, V.M. Shyvaniuk, and S.M. Teus, Electron Concept of Hydrogen Embrittlement and Hydrogen-Increased Plasticity of Metals, *Progress in Physics of Metals*, **25**, No. 3: 482–519 (2024)

1. Introduction

Hydrogen embrittlement (HE) of iron and steel was detected in 1874 by Johnson, who published the results of his observations in 1875 [1]. Hirth and Johnson [2] defined it as the degradation of mechanical properties in metallic materials plastically deformed under the atmosphere of gaseous hydrogen, namely, hydrogen environmental embrittlement (HEE). The same effect occurring in the case of hydrogen after its prior dissolution in a crystal lattice was designated as internal hydrogen embrittlement (IHE). Both kinds of hydrogen-assisted premature fracture were described, possibly, first time, by Louthan [3], and Bernstein and Garber [4], respectively.

This effect is reversible, and the embrittlement disappears, if hydrogen is evacuated from specimens before mechanical tests. A particular feature is manifestation of it in a certain range of temperatures (see, *e.g.*, Refs. [5–8]) and strain rates (see, *e.g.*, Refs. [6–9]). The latter distinguishes hydrogen embrittlement from stress corrosion cracking (SCC).

Several hypotheses have been proposed for interpretation of this rather complicated phenomenon: those of hydrogen pressure expansion (see Refs. [10–12]); hydrogen surface adsorption [13, 14]; hydrogen-induced lattice embrittlement [15, 16]; hydrogen-enhanced decohesion (HEDE) [17–20]; adsorption-induced dislocation emission (AIDE) [21–23]; hydrogen-enhanced strain-induced vacancies (HESIV) [24–26]; nanohydride embrittlement [27–29] and hydrogen-enhanced localized plasticity (HELP) [30–36].

Two of them, HEDE and HELP, are the most common. A central point of the HEDE model proposed in 1972 by Oriani [17] is the hydrogen-caused weakening of interatomic forces at the tip of an existing crack provided a normal stress orthogonal to the crack plane occurs. Due to this stress, the interatomic bonds are broken atom by atom, resulting in continuous crack propagation. A fundamental feature of Oriani's model in its original version is the negation of any role of dislocations in hydrogen embrittlement.

The HELP model, first substantiated by Birnbaum and Sofronis [30] (see also article by Sofronis and Birnbaum [37]), is based on hydrogens' redistribution within its dislocation atmospheres. It occurs due to a linear superposition of stress fields around neighbouring dislocations. Consequently, the repulsion force exerted by neighbouring dislocations decreases, which in turn reduces the applied stress needed to move dislocations with their hydrogen atmospheres. The hydrogen-increased velocity of dislocations and the hydrogen-decreased distance between dislocations in their planar ensembles have been confirmed in several *in situ* TEM observations; see, *e.g.*, those performed by Ferreira *et al.* on 310S stainless austenitic steel [38] and high-purity aluminium [39].

It is worth noting that hydrogen-caused shielding of repulsion between neighbouring dislocations was found only in the calculations for edge dis-

locations. It was also supposed by Ulmer and Altstetter [40] that hydrogen decreases the ability of edge dislocations to cross-slip, thereby assisting slip planarity. This idea was supported by TEM studies of dislocation character in aluminium [39], where hydrogen atoms were shown to stabilize the edge segments of dislocations thereby inhibiting their cross-slip.

Within the last two decades, attempts have been made to bring the HEDE and HELP models together. The HEDE + HELP model follows the earlier cycle of research performed by Gerberich *et al.* [41–43], who substantiated the necessity of both plasticity and brittleness in hydrogen-caused microcracking. The key points of this model are as follow (see, *e.g.*, Djukic *et al.* [44–46]): (i) normal stress in front of the crack tip is obligatory and consistent with the original HEDE model; (ii) hydrogen-enhanced dislocation mobility only prepares the necessary conditions for HEDE to be activated and is substituted by the hydrogen-impeded mobi-lity of dislocations, thereby facilitating HEDE; (iii) above a certain criti-cal hydrogen concentration at the crack tip, the HELP mechanism is replaced by HEDE, which becomes an independent mechanism of hydrogen embrittlement.

The HELP-mediated HEDE model, first proposed at first by Nagao *et al.* [47–49] for quasi-brittle fracture of martensitic steels, also implies the HELP phenomenon as a preliminary stage to the HEDE mechanism. Finally, the intergranular fracture of lath martensitic steel was attributed to the slip of dislocations encased in their hydrogen atmospheres within martensitic blocks surrounded by high-angle grain boundaries and piled up against prior austenitic grains. In contrast, transgranular failure was claimed to occur, if these dislocations are piled up against lath/block boundaries. This model was supported by subsequent studies of intergranular fracture in pure nickel and AISI 316 austenitic stainless steel performed by Bertsch *et al.* [50] and Nygren *et al.* [51], respectively.

It is relevant to note that intergranular fracture in metals can be also interpreted in terms of the above-mentioned HESIF model as the effect of hydrogen-induced superabundant vacancies segregated at grain boundaries, decreasing their strength, which does not require any involvement of dislocations. Consistently with such interpretation, Harris *et al.* [52] observed the intergranular fracture of pure nickel during its tensile tests with hydrogen segregated at grain boundaries before plastic deformation.

This paper aims to analyse the hydrogen effect on the mechanical properties of metallic materials in terms of hydrogen-changed electron structure resulting in hydrogen embrittlement or hydrogen-improved plasticity.

2. Hydrogen Effect on the Electron Structure of Metals

Any applied mechanical force shifts atoms in metals from their positions, and the response of crystal lattice, plastic deformation or brittle fracture, is controlled by the type of interatomic bonds. The closed electrons' shell

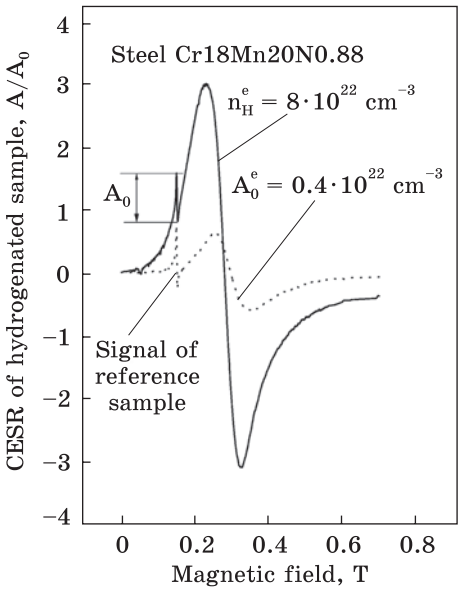

Fig. 1. Conduction electron spin resonance (CESR) in the hydrogen-free (dashed line) and hydrogen-charged (solid line) steel Cr18Mn20N0.88. The CESR signal is recorded as a derivative of the absorbed microwave power on the external magnetic field. The area under CESR signal is proportional to the concentration of free electrons. Measurements were performed at 77 K. Signal A_0 belongs to the reference sample (borate glass) containing 10^{15} electron spins and is seen on the left side of the main CESR signal. According to Shanina *et al.* [53]

of ion is only slightly polarized under strain and does not take part in this response. The relaxation time of valence electrons is shorter by several orders of magnitude in comparison with that of the ion shell. Therefore, only valence electrons forming interatomic bonds are responsible for the character of deformation behaviour. Their prevailing localisation at atoms with narrow electron bridges between them creates covalent interatomic bonds and causes brittleness, as is the case in groups V and VI of metals in the periodic table (V, Nb, Ta, Cr, Mo, W), where only the so-called bonding electron states in the d-electron band are filled. In contrast, in metals where the bonding states in the *d*-electron band only start to be filled, *e.g.*, Ti in group IV and from Fe to Cu in groups VIII to XI with the essentially filled antibonding electron states, the prevailing free electrons promote ductility. They are responsible for the so-called metallic character of interatomic bonds, and therefore the ductility of metals and their alloys is the higher, the larger the fraction of free electrons.

Using the conduction electron spin resonance (CESR), the first experimental study of the hydrogen effect on the electron structure of steels was performed by Shanina *et al.* in 1999 [53]. Shown in Fig. 1, there is the CESR spectrum of the hydrogen-charged stainless austenitic steel that is not ferromagnetic at any low temperatures.

Thus, hydrogen in austenitic steels significantly increases the concentration of free electrons, enhancing the metallic character of interatomic bonds and thereby increasing ductility in steels.

A reason for that was clarified through the first principles calculations of the electron structure [54, 55, 57] using the density functional

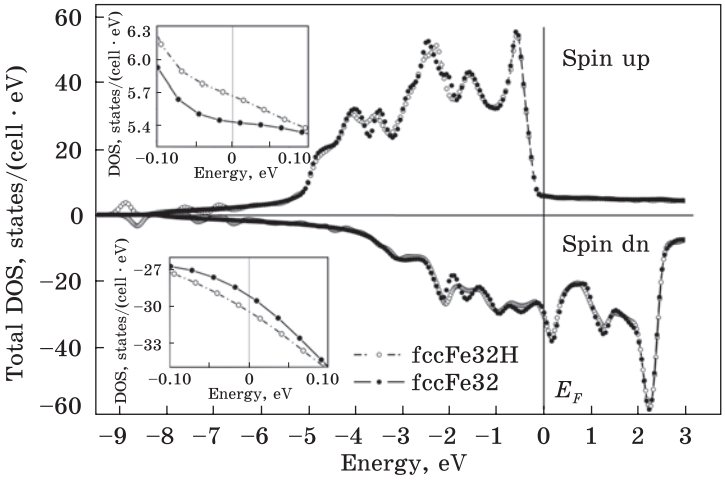

Fig. 2. DOS for f.c.c. iron without (solid line) and with (dashed line) hydrogen at the atomic ratio, H/Fe, of 1/32 for two orientations of electron spins under applied magnetic field. The insets on the left show the density of states at the Fermi level E_F. Adopted from Ref. [57]

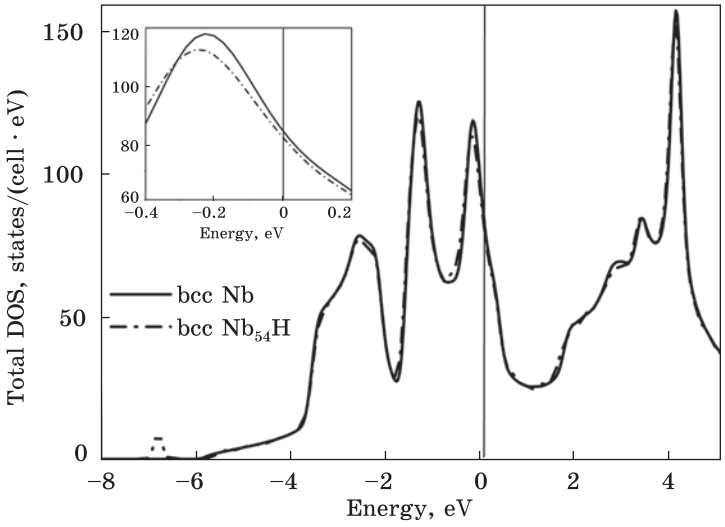

Fig. 3. DOS in the niobium hydrogen-free (solid line) and hydrogen-doped (dashed-dot line) at the atomic ratio $H/M = 1/54$. DOS in the vicinity of Fermi level is presented in the inset. Adopted from Ref. [57]

theory and program package Wien-2k. The density of electron states (DOS) in the *d*-zone of transition metals, particularly, at the Fermi level, was the object of these studies.

As shown in Fig. 2 for f.c.c. iron, hydrogen increases the density of electron states at the Fermi level, which is proportional to the concentration of free electrons.

Table 1. **Total DOS at the Fermi level in hydrogen-free and hydrogen-containing metals at different size of calculated cells and corresponding hydrogen/metal (H/*M*) atomic ratios**

Metal	H/*M* ratio	Total DOS, states/(eV·cell)
b.c.c. iron	H-free	46.69
	1/54	50.85
f.c.c. iron	H-free	34.11
	1/32	36.20
nickel	H-free	55.18
	1/32	56.42
	3/32	62.10
	6/32	64.85
	16/32	55.54
	32/32	25.22
b.c.c. titanium	H-free	4.278
	1/2	4.699
	1/1	3.348
	2/1	1.677

Table 2. **Calculated data for DOS at Fermi level per atomic cell in b.c.c. Nb**

System and *M*/H ratio	DOS at Fermi level, states/(eV·cell)
Nb (H-free)	83.76
NbH (54/1)	81.3

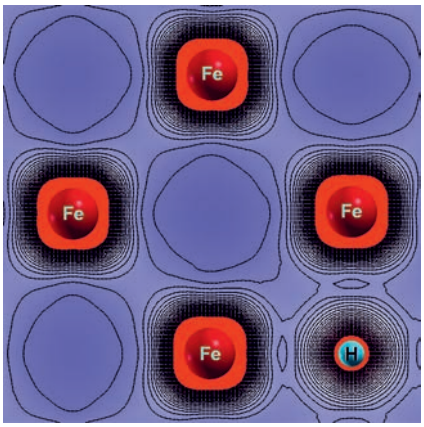

Fig. 4. Top view of the spatial distribution of valence electrons on the atomic plane (002) throughout the f.c.c.-Fe lattice at the H/Fe ratio of 1/32. H atoms are located in the octahedral sites. Adopted from Ref. [144]

Such calculations have been also carried out for the b.c.c. Fe, f.c.c. Ni, and b.c.c. Ti. The obtained data are presented in Table 1.

In all the studied metals, hydrogen increases the DOS at the Fermi level. The dependence of DOS on hydrogen concentration in nickel and titanium is non-monotonous because of a miscibility gap in the Ni–H solid solution (see Ref. [56]), and the formation of titanium hydrides [57].

It is remarkable that, before some critical concentration in the hydride forming titanium, hydrogen increases the DOS. Quite different is the hydrogen effect in the strong hydride-formers (see, *e.g.*, Fig. 3 and Table 2 for the DOS in the hydrogen-containing niobium).

As follows from comparing Tables 1 and 2, hydrogen decreases the DOS at the Fermi level in niobium and, consequently, it is expected decreasing the concentration of free electrons at its significantly smaller concentration in comparison with those in titanium.

An example of the spatial distribution of valence electrons over the crystal lattice is presented in Fig. 4 for hydrogen-containing f.c.c.-Fe.

It follows from these data that hydrogen atoms are acceptors of electrons and the concentration of free electrons is increased in their neighbourhood.

As will be shown in the following, the analysis of the hydrogen effect on the atomic level interactions in metals allows proposing the electron basis for the HELP phenomenon, different from the one developed within the framework of continuum mechanics.

3. Localization of Plastic Deformation and Short-Range Atomic Order

Although included in its acronym, the hydrogen-enhanced localization of plastic deformation is not really elucidated by the HELP theory.

The oft-recurring statements are as follow (see, *e.g.*, Refs. [58–60]): (i) hydrogen can promote localization of homogeneous macroscopic plastic deformation into the bands of intense shear; (ii) inhomogeneous hydrogen distribution causes the flow stress to be lower in areas where the hydrogen concentration is the highest; (iii) if a solid solution is hardened due to formation of hydrides or the hydrogen clusters, the initial passage of dislocations by cutting through these obstacles reduces the stress for continued slip in the same shear band; (iv) hydrogen-induced volume dilatation can cause shear localization even with uniform hydrogen distribution.

It is worth noting that no shear bands are observed in pure metals, *e.g.*, in iron, nickel and aluminium, whatever hydrogen is present or not. Their observation by Hwang and Bernstein in hydrogen-charged iron single crystals [61] (as well as by Le and Bernstein in hydrogen-charged spheroidized steel [62]) relates to Si-rich particles cut by dislocations in the former case and with localized dislocation structure emanating from carbide particles in the latter one. The cutting of precipitates by the first moving dislocations eases the passing of the subsequent ones in the vicinity of the same planes.

The hydrogen-enhanced waviness of dislocation slip in deformed nickel was found by McInteer *et al.* [63]. The prevailing formation of dislocation cells was also observed by Wang *et al.* [64] in the hydrogen-charged pure nickel subjected to high-pressure torsion. Harris *et al.* [52] did not reveal a systematic difference in either dislocation-cell size or dislocation–grain boundary interactions between the structures in uncharged or hydrogen-charged pure nickel subjected to plastic deformation. According to Bertsch *et al.* [50], hydrogen also intensifies the formation of a cell dislocation structure in nickel during uniaxial tensile deformation. However, these authors observed slip microbands depending on the grain orientation.

There is also no clear evidence of the shear bands in pure aluminium. It occurs in the hydrogen-free Al–Li alloys because of cutting the Al_3Li precipitates by dislocations (see, *e.g.*, Ref. [65]), and disappears, if the size of precipitates is too large for their cutting [66]. Hydrogen in these alloys causes a prevailing intergranular fracture (see, *e.g.*, Ref. [67]).

Conceivably, the hydrogen-caused localization of plastic deformation in pure metals can be related to hydrogen-induced superabundant vacan-

cies. These vacancies were predicted in theoretical calculations for solid solutions containing any interstitial elements searching for interpretation of a decrease in the activation enthalpy of self-diffusion with increasing carbon content in iron, as detected by Gruzin [68].

The first thermodynamic analysis in this respect was performed in 1988 by McLellan [69], who reported a carbon-caused five-fold increase of vacancy concentration in the f.c.c. Fe–C solid solution with the carbon content $\theta_C = n_C/N_{Fe} = 0.06$. Similar results were obtained in the theoretical calculations carried out in 1991 by Smirnov for any interstitial atoms [70]. Later on, Carr and McLellan [71] described the formation of H–vacancy clusters in Pd, Ni, Fe, Mo, and Nb.

The first experimental evidence of superabundant vacancies induced in Ni and Pd under high hydrogen pressure was obtained in 1993 by Fukai and Okuma [72] using *in situ* measurements of x-ray diffraction. The hydrogen-induced vacancies in austenitic steel were first demonstrated by Gavriljuk *et al.* [73] in 1996 using transmission electron microscopy.

Later on, the hydrogen-increased concentration of vacancies and the formation of hydrogen–vacancy complexes were analysed, using the first principles calculations, by Takeyama and Ohno [74], Counts *et al.* [75], Nazarov *et al.* [76], Lu and Kaxiras [77].

Takeyama and Ohno [74] found stable vacancy–hydrogen atomic configurations VH_2 in b.c.c. iron and demonstrated the formation of line-shape vacancy clusters along atomic planes typical of hydrogen-caused brittle fracture of steels. As obtained by Nazarov *et al.* [76], a vacancy in f.c.c. iron can be occupied by up to six H atoms. A feature of hydrogen in aluminium is that a single vacancy can trap up to 12 hydrogen atoms (see article by Lu and Kaxiras [77]).

According to Birnbaum *et al.* [78], H–vacancy complexes in aluminium form platelets of about 15 nm in radius and 7 nm in thickness, which lie on the planes (111). If so, the hydrogen-induced vacancies can act as microvoids, and, as consistent with the 'voids' sheeting' model proposed by Teirlinck *et al.* [79], one may suggest a decrease in dA_b/A_b in the load-bearing area along these atomic planes leading to the formation of shear bands:

$$\frac{dA_b}{A_b} = -4r_v^3 N_v d\gamma \,, \qquad (1)$$

where A_b is the slip area, r_v is the void radius, and N_v is the void density per unit volume.

As evidence of localized plastic deformation, the formation of hydrogen-assisted shear bands is certain in solid solutions, *e.g.*, in the martensitic and austenitic steels (see Refs. [35, 38]), respectively. A widely shared idea for their interpretation is associated with hydrogen-decreased stacking fault energy (SFE) expected to inhibit the cross slip of dislocations

thereby assisting its planarity, although, it is not clear why planar slip on its own can result in the formation of separate slip bands. The uncertainty of the SFE concept can be clearly demonstrated by comparing different dislocation substructures in the cold-worked carbon and nitrogen austenitic steels.

Both carbon [80, 81] and nitrogen [82] are known to increase SFE in austenitic steels, although, some decrease of SFE is observed at high nitrogen contents. Nevertheless, at any concentration, carbon assists the formation of a tangled dislocation structure during cold work (see, *e.g.*, Ref. [83]), whereas nitrogen facilitates planar dislocation slip and localizes plastic deformation into shear bands [83, 84].

Closer to explaining the hydrogen-enhanced localization of plastic deformation is short-range atomic order (SRO) observed in solid solutions and firstly analysed by Gerold and Karnthaler [85] as a main reason for planar slip in f.c.c. alloys.

Cowley was the first to describe atomic distribution in solid solutions in terms of interaction between solute atoms of different kinds (see Ref. [86]). The nearest neighbourhood of A and B atoms in the AB solid solution is characterized by Cowley's parameter α:

$$\alpha = 1 - P_{lmn}/c_A \,, \tag{2}$$

where P_{lmn} is the probability that an atom with (l, m, n) co-ordinates concerning a B atom in the coordinates' origin should be an A atom, c_A is the atomic fraction of the A atoms in a binary solid solution with $c_A + c_B = 1$. P_{lmn}/c_A is equal to the atomic ratio $N_{AB}^{\text{real}}/N_{AB}^{\text{ideal}}$ between the number N of atomic pairs AB in actual and ideal binary solid solutions.

Therefore, two types of SRO are possible. A preference in the nearest neighbourhood for different kinds of atoms, A–B, or for the same kind, A–A and B–B, is denoted as short-range atomic ordering or short-range atomic decomposition of solid solutions with $\alpha < 0$ and $\alpha > 0$, respectively.

Short-range atomic order in substitutional solid solutions was studied in detail summing up available experimental data back in the seventies of the last century [87, 88]. The miscibility gap observed in b.c.c.-Fe–Cr alloys results in the formation of chromium-rich and iron-rich submicrovolumes [89]. At the same time, the short-range ordering was detected in these alloys at small chromium contents [90]. Manganese is shown to form atomic clusters in f.c.c. Fe–Mn alloys [91, 92]. According to first-principle calculations [93], the Fe–Fe and Ni–Ni neighbourhoods prevail in comparison with the Fe–Ni one within the Fe–Ni alloys. Superstructures Fe_3Ni, FeNi and $FeNi_3$ were analysed in several studies, *e.g.*, [94, 95], making it possible to suggest that short-range decomposition of binary FeNi alloys is accompanied by atomic ordering in the areas rich with nickel.

Using energy-dispersive x-ray analysis, Garner and McCarthy [96] studied atomic redistribution in the Fe–Ni and Fe–Ni–Cr invar alloys un-

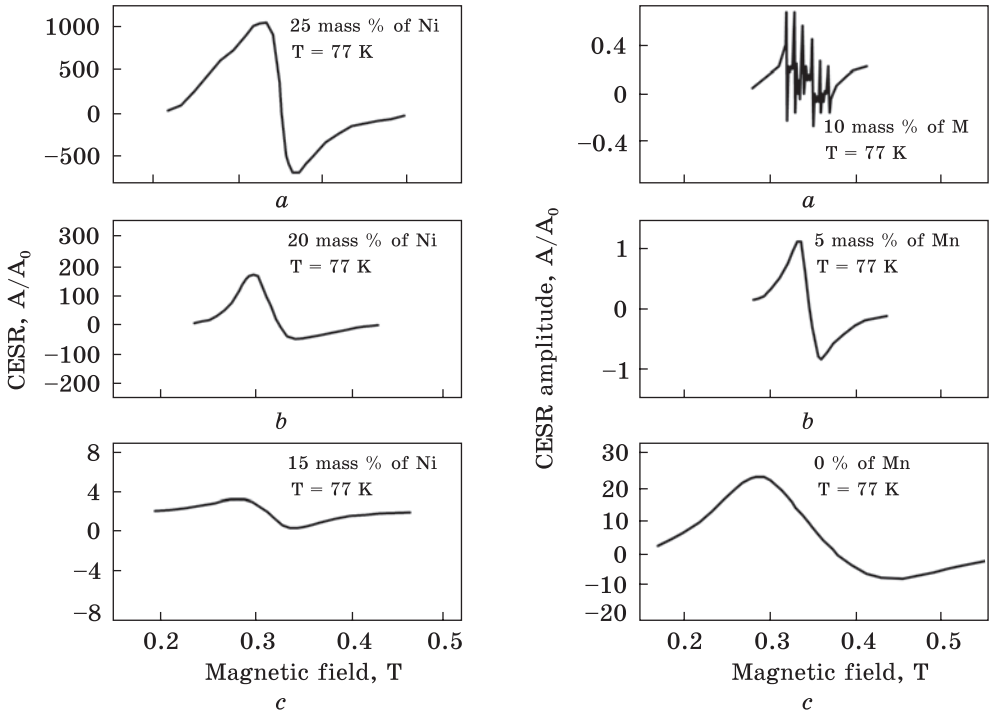

Fig. 5. Conduction electron spin resonance in steels Cr15Ni15 (*a*), Cr15Ni20 (*b*), and Cr15Ni25 (*c*). Adopted from Ref. [102]

Fig. 6. Conduction electron spin resonance in Cr15Ni20 (*a*), Cr15Ni20Mn5 (*b*), and Cr20Ni20Mn10 (*c*) steels [102]

der electron- and neutron-irradiation at elevated temperatures. The authors obtained that both kinds of alloys are decomposed in a spinodal-like manner forming Fe- and Ni-rich areas with nickel-level oscillations between 25% and 50% and wavelengths of 100 nm to μm. Chromium behaviour was found to be similar to that of iron. Rotman *et al.* [97] also observed a similar short-range decomposition of a Fe–45Ni–16Cr alloy after 1 MeV electron irradiation at 500 °C.

The role of irradiation amounts merely to an increase in the concentration of vacancies and self-interstitial atoms, which accelerates the diffusion of metallic atoms. The inherent thermodynamic nature of short-range decomposition has been proven by Wiedenmann *et al.* [98], who detected oscillating fluctuations of Ni concentration between 28.5 and 36.5 at.% at temperatures of 625 to 725 °C in a Fe–34 at.% Ni alloy. The spatial extent of these fluctuations exceeded 200 nm. It is presumably that chemical inhomogeneity can remain after solution treatment.

A correlation between short-range atomic order and electron structure in the iron-based solid solutions was studied in Refs. [99–102] (see Figs. 5 and 6 along with Table 3).

Adding nickel increases the concentration of free electrons in CrNi austenitic steel, whereas manganese and chromium decrease it. Instead of CESR, the electron paramagnetic resonance (EPR) from not compensated electrons at the Mn atoms with a well-resolved hyperfine structure is observed in steel Cr20Ni20Mn10. Six lines belong to ^{55}Mn atoms with the nuclear spin $I = 5/2$. The measured value of the constant of hyperfine splitting $A = 93.3 \cdot 10^{-4}$ cm^{-1} is typical of paramagnetic atoms Mn^{++} in the solid-state compounds with a cubic symmetry of the crystalline field (see, *e.g.*, Ref. [103]).

Based on the data of contributions to magnetic susceptibility from different electron subsystems, namely free electrons, single atoms of *d*-elements with not compensated electrons and superparamagnetic clusters, *i.e.*, atomic clusters of *d*-elements, a tendency to form clusters in multicomponent iron-based solid solutions was studied in Refs. [99–102]. This analysis used a difference in the temperature dependence of magnetic susceptibilities caused by the mentioned electron subsystems. The temperature dependence of a relative magnetic susceptibility $\chi_r^{-1} = \chi_f/\chi_d$ with those of free electrons, χ_f, and not compensated electrons localized on the atoms with the not filled *d* band, χ_d, is described by the following formula (for details, see Refs. [101, 102]):

$$\chi_r^{-1}(T) = \alpha_1\chi_{f0} + \chi_{f0}\chi_{d1}^{-1} + \alpha_2\chi_{d2}\chi_{f0}\chi_{d1}^{-1}, \qquad (3)$$

where α_1 is a parameter of the exchange interaction between the free electrons and those localised on the single atoms of *d*-elements, χ_{f0} is the magnetic susceptibility of free electrons which does not depend on temperature, χ_{d1} is the magnetic susceptibility of single atoms of *d* elements, which obeys the Curie law $\chi_{d1}(T) = C_1/T$, α_2 is a parameter of the exchange interaction between the free electrons and superparamagnetic atomic clus-

Table 3. **Concentration of free electrons n_0, clustering coefficient K_c, and correlation between the interatomic bonding types and SRO in austenitic steels**

Alloy	n_0, 10^{22} cm^{-3}	K_c	Varying element	Enhanced bonds	Assisted SRO
Cr15Ni15	0.14	378	—	—	—
Cr15Ni20	0.37	5.3	Ni	metallic	ordering
Cr25Ni25	0.10	254	Cr	covalent	clustering
Cr15Ni20Mn5	0.16	42	Mn	covalent	clustering
Cr15Ni20Mn10	0.09	—	Mn	covalent	clustering
Cr15Ni20Mo1.3	0.09	84	Mo	covalent	clustering
Cr25Ni20Cu2.5	0.31	71	Cu	metallic	ordering
Cr18Ni16Mn10 (0.4N)	2.6	19	N	metallic	ordering
Cr18Ni16Mn10 (0.3C)	0.19	4.9	C	covalent	clustering

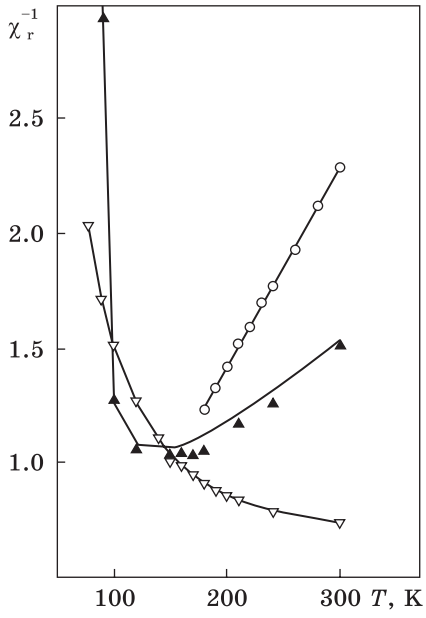

Fig. 7. Temperature dependence of the relative magnetic susceptibility $\chi_r^{-1} = \chi_f/\chi_d$ for austenitic steels Cr15Ni25 (circles), Cr15Ni20 (open triangles) and Cr15Ni20Mo1.3 (closed triangles). For convenience, the data for steel Cr15Ni25 are increased by 10 times. Decrease in the nickel content and alloying with molybdenum cause non-monotonous temperature behaviour of χ_r^{-1}, which is a sign of the tendency to clustering [101]

ters of d elements, χ_{d2} is the magnetic susceptibility of the superparamagnetic cluster, which obeys the Langevin law $\chi_{d2}(T) = C_2 L(\theta/T)$ with $C_2 = \chi_{d2}$ at $T = 1$ K, $L(\theta/T) = \coth(\theta/T) - T/\theta$, $\theta = MH/k_B$, where M is the magnetic moment of the cluster, H is the external magnetic field, k_B is the Boltzmann constant, θ is the energy of cluster under magnetic field in temperature units, which is proportional to the number of atoms in the cluster.

The temperature dependence of χ_r^{-1} is shown in Fig. 7 for three austenitic steels. In the absence of superparamagnetic clusters, $\chi_r^{-1}(T)$ should be a linear function of temperature.

It is seen that clustering is enhanced, if the nickel content in CrNi steel decreases or if this steel is additionally alloyed with molybdenum.

The clustering tendency in the multicomponent solid solutions of 3d transition metals can be characterized by the following parameter (see Ref. [102]):

$$K_c = \alpha_2 C_2 \theta/\alpha_1 C_1. \quad (4)$$

Following Eq. (3) and Fig. 7, $\alpha_2 C_2$ is proportional to the number of atomic clusters in the sample, and θ is proportional to the number of atoms in the cluster; therefore, their product characterises the number of atoms included in the cluster system. The $\alpha_1 C_1$ is proportional to the number of single atoms of d-elements in the solid solution. If the value of K_c is higher, the clustering is stronger. Data on the correlation between interatomic bonds and a type of SRO are presented in Table 3 for several austenitic steels (see Ref. [101]).

Thus, nickel in austenitic steels assists the short-range atomic ordering, whereas chromium, manganese and molybdenum promote clustering.

A unique possibility to bring to light the short-range atomic order in multicomponent solid solutions is provided by measurements of stacking fault energy that is controlled by chemical compositions of metallic materials (see Fig. 8 and [104] for details).

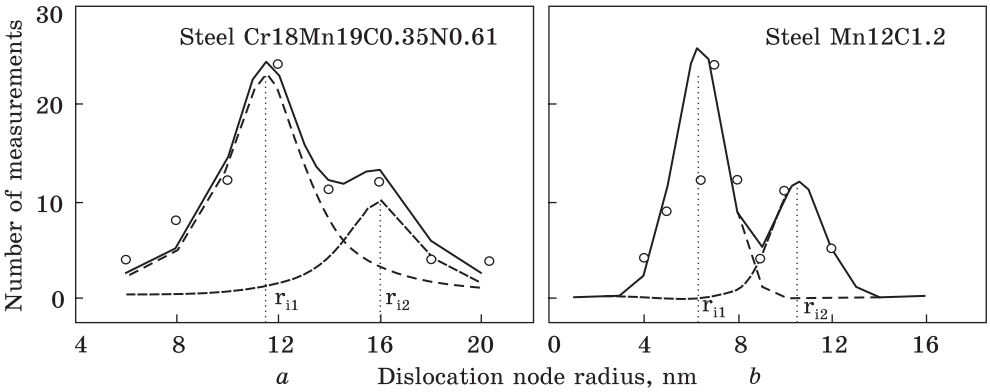

Fig. 8. Frequency curves of the measured dislocation triple node radius in Cr18Mn19 (*a*) and Mn12C1.2 (*b*) austenitic steels. Adopted from Shanina *et al.* [104]

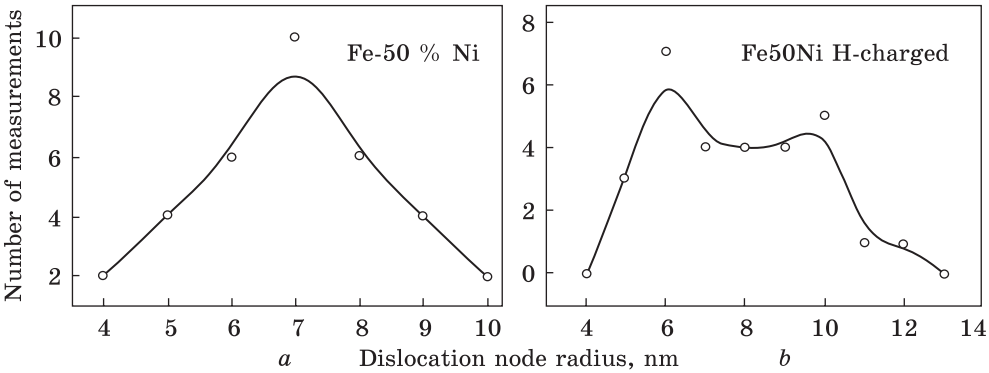

Fig. 9. Triple nodes in the previously solution treated alloy Fe50Ni50 before (*a*) and after (*b*) hydrogen charging. According to Ref. [104]

Table 4. **Dislocation triple node radius, r_i, and SFE**

Steel	r_1, nm	r_2, nm	SFE_1, mJ/m^2	SFE_2, mJ/m^2	DSFE, mJ/m^2
CrMnCN	11.5	16.0	38	27	11
MnC	6.4	10.6	68	41	27

The fitting of the experimental data was carried out using a Gauss distribution, which is natural for the statistical scattering in the experimental data. The obtained SFE values are presented in Table 4.

Two maxima of dislocation splitting give evidence of short-range decomposition in the studied steels and the existence of submicrovolumes having different chemical compositions. One can see that the gap between them is smaller in the C+N steel, where combined alloying by carbon and nitrogen is known to increase concentration of free electrons assisting

ordering (see Refs. [84, 104]), whereas it becomes clearly apparent in the Hadfield-type carbon steel with Mn–C, where carbon promotes covalent interatomic bonds and corresponding clustering.

It is worth noting that, due to the different chemical affinity of hydrogen with elements constituting metallic alloys and its significant effect on the stacking fault energy, hydrogen can serve as an appropriate tool for the identification of short-range atomic order in solid solutions, where it is not clearly detectable using an available experimental technique. As an example, the occurrence of short-range atomic decomposition in the equiatomic FeNi-alloy solution treated at 1000 °C is demonstrated in Fig. 9.

Along with the hydrogen effect on the line tension of dislocations, their velocity in the submicrovolumes of different chemical compositions of short-range decomposed solid solutions is expected to be controlled by their different hydrogen-caused splitting. In the case of short-range atomic ordering, as mentioned above, its local destruction by first gliding dislocations makes it easy to slide the subsequent ones resulting in the formation of the slip bands. Because of the increased concentration of free electrons within the hydrogen atmospheres at dislocations and a corresponding increase in their velocity, hydrogen assists this phenomenon.

As obtained by Movchan *et al.* [93] in their calculations of interatomic bonds in the binary FeNi solid solutions, the Fe–Fe and Ni–Ni bonds prevail over the Fe–Ni one, which is consistent with a spinodal-like decomposition measured by Garner and McCarthy [96]. Moreover, according to Ref. [93], hydrogen atoms prefer the neighbourhood of the iron, rather than nickel atoms. This suggests higher hydrogen solubility in the iron-rich submicrovolumes leading to higher velocity of dislocations so that plastic deformation is localized there.

Thus, one can state that hydrogen itself is not responsible for the localization of plastic deformation, which is inherent in metallic alloys if the short-range atomic order becomes sufficiently apparent. Hydrogen merely enhances it because of increased velocity of dislocations.

4. Hydrogen Embrittlement and Increased Plasticity

As follows from the hydrogen effect on the electron structure of metals, hydrogen atmospheres around the dislocations in pure iron or nickel and titanium at sufficiently low hydrogen contents are characterized by the increased concentration of free electrons and, consequently, by the decreased shear module μ with the following consequences for dislocation properties:

• a decrease in the critical stress for activation of dislocation sources, *e.g.*, $\sigma \gg 2\mu b/L$ for the Frank–Reed dislocation source with L as a distance between the pinning points, which decreases the yield stress under mechanical loading easing, thereby, the start of plastic deformation;

• a decrease in the specific energy of dislocations, namely their line tension $\Gamma \gg (\mu b^2/4\pi)/\log(\hat{A}/5b)$ with $\hat{A}$ as the dislocation curvature radius, which results in the increased velocity of dislocations whatever they are edge or the screw ones;

• a decrease in the distance between dislocations in their planar ensembles resulting in the increased shear stress at the leading dislocation, $\tau_L = n\tau$, where τ is applied stress and τ_L is the leading dislocation, resulting, thereby, in the earlier opening of a microcrack ahead of the pile-ups.

These are those phenomena, which have been observed in the experimental studies confirming the HELP theory. Nevertheless, some distinctive features are worth to be noted. First, within the electron concept, hydrogen changes the properties of individual dislocations, not the interaction between them. Second, in contrast to the shielding effect predicted by the HELP theory for edge dislocations, both the screw and edge ones acquire the increased velocity due to the enhanced metallic character of atomic bonds within the dislocation atmospheres. Third, hydrogen should increase plasticity of metallic alloys provided that deviations from the random atomic distribution in the solid solution are not significant or if the interaction between hydrogen atoms and dislocations is rather weak.

Let us analyse available experimental data about hydrogen effect on the mechanical properties of metallic materials in terms of the electron concept of hydrogen brittleness in comparison with the HELP theory.

4.1. Hydrogen-Increased Velocity of Dislocations

The strain-dependent internal friction (SDIF) caused by the strain-induced alternating movement of dislocations is a simple and reliable means of estimating dislocation mobility, because, at a constant frequency of mechanical vibrations, their amplitude is proportional to the area swept by dislocations. Presented in Fig. 10, there is SDIF measured in austenitic steel Cr25Ni20 before and after hydrogen charging.

It is seen that hydrogen in this steel decreases the stress needed for dislocation slip and increases dislocation velocity. Hydrogen degassing restores the previous state, except for a small increment of internal friction caused by new dislocations emitted under small-applied stress during cyclic SDIF measurements.

Exactly this hydrogen effect is interpreted within the HELP theory developed in terms of continuum mechanics as a result of the hydro-gen-caused shielding of stress fields created by neighbouring dislocations. A feature of this theory is that hydrogen atoms are presented simply as point defects, which cause elastic stresses in the crystal lattice, whereas the chemical interaction between hydrogen and metallic atoms is ignored.

If so, any interstitial elements in solid solutions should increase dislocation velocity, provided the atmospheres of interstitial atoms accompany

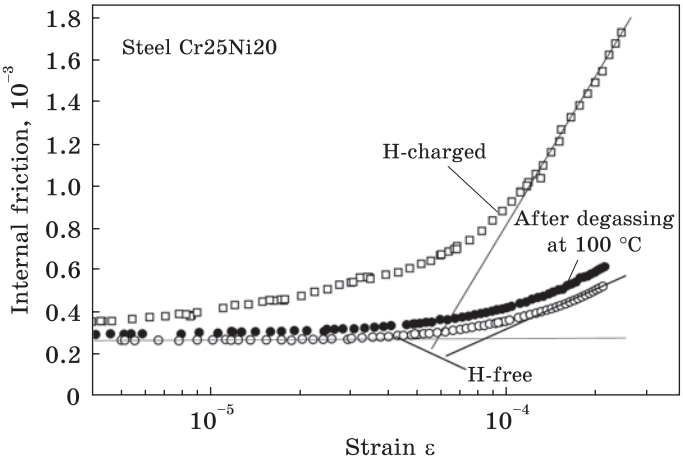

Fig. 10. Hydrogen effect on the strain-dependent internal friction, Q^{-1}, in steel Cr25Ni20: hydrogen-free state (open circles), after hydrogen charging at 50 mA/cm^2 for 48 h (open squares), after subsequent hydrogen degassing at 100 °C (solid circles). Measured at frequency of ≈1 Hz and heating rate of 1.5 K/min. Adopted from Shyvaniuk *et al.* [142]

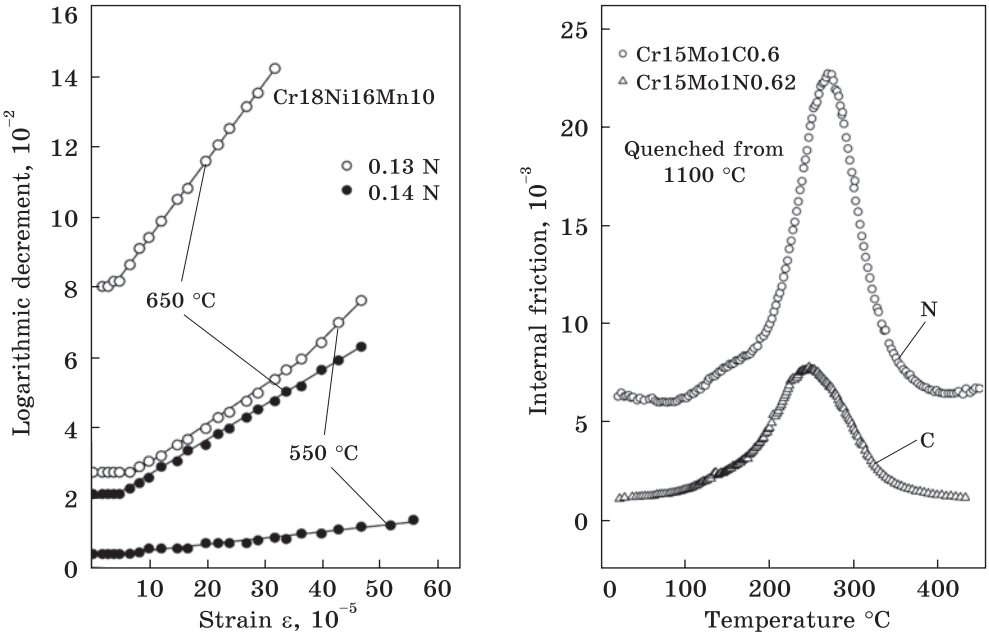

Fig. 11. Strain dependence of internal friction in the carbon and nitrogen austenitic steels. According to Gavriljuk *et al.* [143]

Fig. 12. Snoek–Köster relaxation caused by carbon and nitrogen in martensitic Cr15Mo1C0.6 and Cr15Mo1N0.62 steels [143]

dislocations during plastic deformation. A fitting possibility to test the shielding effect of interstitials on dislocation velocity is provided by nitrogen and carbon in austenitic steels. The point is that their atoms acquire nearly the same effective size in b.c.c. and f.c.c. crystal lattices (see Refs. [101, 105]), respectively, thereby causing similar elastic stresses. There-

fore, the shielding effect is expected to be nearly the same for these elements in iron-based solid solutions and, consequently, dislocation velocities should be comparable.

Strain-dependent internal friction in austenitic Cr18Ni16MN10 steel alloyed with C or N is presented in Fig. 11.

The diffusivity of carbon and nitrogen atoms in f.c.c. iron within the temperature range above 500 °C is sufficiently high. Therefore, they can be transported by dislocations at strains of $\gg 10^{-5}$ and vibration frequencies of $\gg 1$ Hz. As shown in Fig. 11, dislocation velocity in nitrogen austenitic steel significantly exceeds that in carbon one.

The same is true for the nitrogen and carbon effects on dislocation properties in martensitic steels. Snoek–Köster relaxation caused by moving dislocations dragged by interstitial atoms occurs in alloys with b.c.c. crystal lattice. It follows from Fig. 12 that dislocations encased in the atmospheres of nitrogen atoms acquire higher velocity in comparison with that is the case of carbon ones.

Since C and N atoms cause similar distortions in the crystal lattice of iron alloys, the comparison of their effects on dislocation velocity makes it possible to conclude that the HELP theory overestimates the shielding effect of interstitial hydrogen atoms. It is worth noting that a giant Snoek–Köster relaxation in b.c.c.-Fe is caused by hydrogen in comparison with so called α-relaxation caused by the same dislocations in the hydrogen-free iron (see Ref. [106]).

A feature of iron alloys doped with nitrogen or charged by hydrogen is the increased concentration of free electrons. Thus, the hydrogen-enhanced metallic character of interatomic bonds resulting in the decrease of the shear module is the real reason for the decrease in the line tension of dislocations and, consequently, their increased mobility.

4.2. Hydrogen–Dislocation Interaction and Temperature Range of Hydrogen Embrittlement

Cottrell and Bilby [107] described the interaction between dislocations and interstitial atoms with the following equation:

$$c = c_0 \exp\left(\frac{\beta \sin\theta}{r k_B T}\right), \tag{5}$$

where c_0 is a concentration of solute atoms at distances of r from a dislocation, and β is proportional to the difference between the host atomic volumes and solute atoms in the solid solutions.

Transforming this formula, one can obtain the relation between hydrogen concentrations in the bulk and at dislocations using the Arrhenius equation

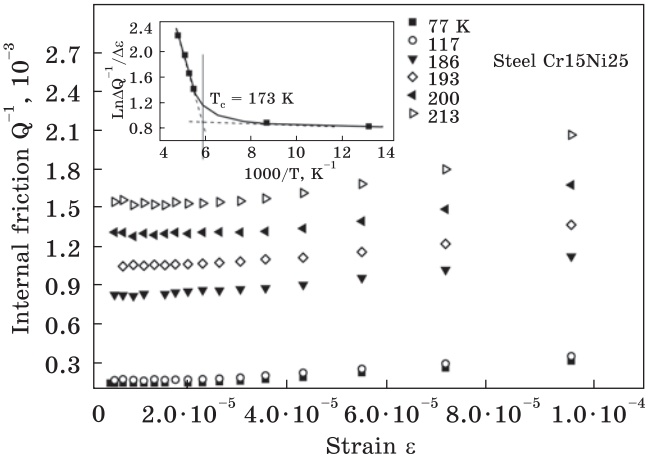

Fig. 13. Strain-dependent internal friction in the hydrogen-charged Cr15Ni25 steel at different temperatures. Treatment of experimental data in the Arrhenius coordinates as $\ln(\Delta Q^{-1}/\Delta\varepsilon) = f(T^{-1})$ is shown in the inset. The ratio $\ln(\Delta Q^{-1}/\Delta\varepsilon)/K^{-1} = H_b/k_B$. According to Teus *et al.* [145]

$$c_\perp = c_0 \exp\left(\frac{H_b}{k_B T}\right), \tag{6}$$

where c_0 and $c_\perp$ are hydrogen contents in the bulk and at dislocations, respectively, H_b is the enthalpy of binding between hydrogen atoms and dislocations.

Measurements of strain-dependent internal friction at different temperatures make it possible to study hydrogen–dislocation interaction in terms of binding enthalpies [57, 108] (see Table 5 and, *e.g.*, experimental data for hydrogen effect on dislocation mobility in austenitic steel Cr15Ni25 in Fig. 13).

At 77 and 117 K, the H atoms are 'frozen'. They serve as point obstacles to moving dislocations remaining practically immobile. At higher tem-

Table 5. **Effect of chemical compositions on the enthalpy of binding between hydrogen atoms and dislocations, ΔH_b, in comparison with that of diffusion, ΔH_d, and condensation temperatures, T_c. Here are presented the data for austenitic steels [54], Ni [109, 110], Inconel 718 [111], β-Ti alloy [112], b.c.c. Fe [113, 114]**

Alloy	$H_b \pm 0.01$, eV	$H_d \pm 0.01$, eV	$T_c \pm 5$, K
FeCr15Ni25	0.11	0.54	173
FeCr15Ni40	0.09	0.49	163
FeCr25Ni25	0.12	0.59	189
FeCr15Ni25Cu2	0.10	0.52	174
FeCr15Ni25Mn15	0.12	0.57	182
b.c.c. Fe	0.28	0.04	—
Ni	≈0.08	0.42	—
Inconel 718	0.07	0.42	149
TiV10Fe2Al3	0.03	0.27	Below 77 K

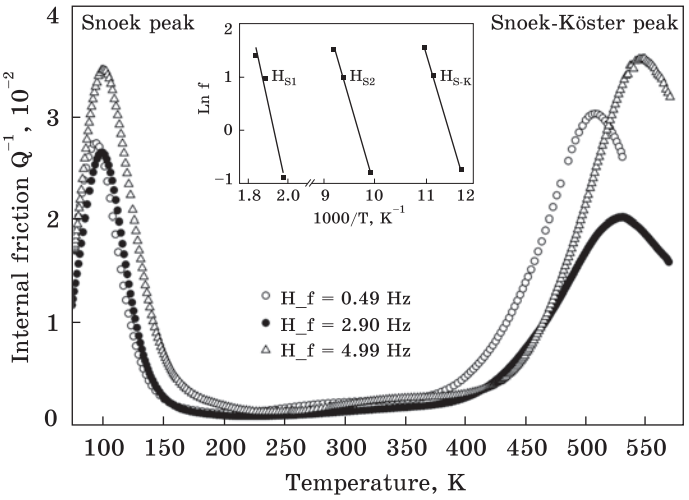

Fig. 14. Snoek-like and Snoek–Köster relaxation peaks in the β-Ti–10V–2Fe–3Al alloy, as measured at different frequencies [145]

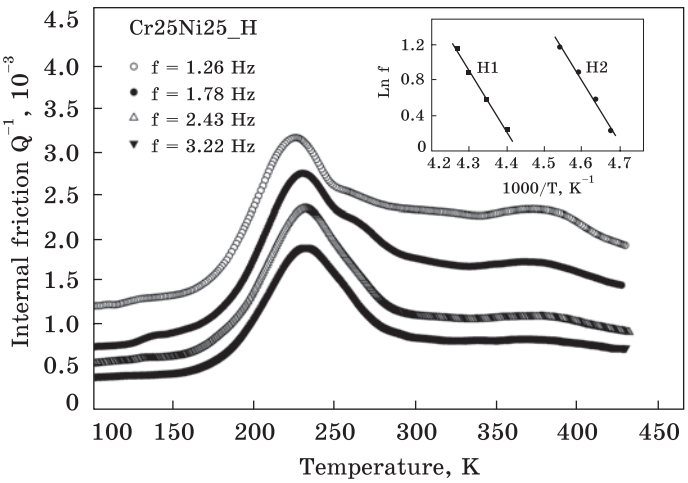

Fig. 15. Hydrogen Snoek-like relaxation in austenitic steel Cr25Ni25. Treatment in the Arrhenius coordinates of the experimental data at temperatures between 150 and 300 K is shown in the inset [145]

peratures, hydrogen atoms acquire diffusivity and can follow dislocations as their hydrogen atmospheres, thereby, increasing internal friction.

Treatment in the Arrhenius coordinates reveals two temperature areas of experimental data for dislocations pinned by hydrogen atoms and for those moving, accompanied by hydrogen atmospheres.

The intersection point between these two branches of the experimental curve is the condensation temperature for hydrogen atoms at dislocations. Hydrogen atmospheres weaken their binding with dislocations above this temperature and become diluted. The ratio $\ln(\Delta Q^{-1}/\Delta\varepsilon)/K^{-1}$ is equal to H_b/k_B, which makes it possible to obtain the enthalpy of hydrogen–dislocation binding.

Its values are presented in Table 5 along with the condensation temperatures and enthalpies of hydrogen diffusion obtained using tempera-

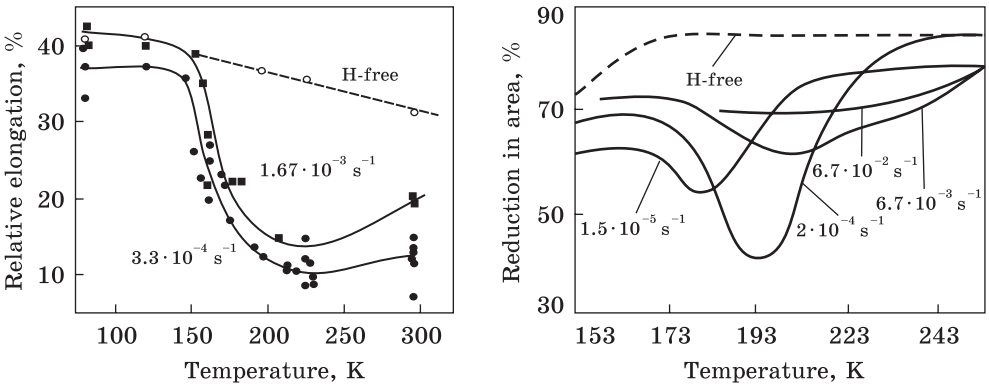

Fig. 16. Relative elongation of hydrogen-free nickel and Ni containing ≈0.2 at.% H at various temperatures. Redrawn from Boniszewski and Smith [6]

Fig. 17. Effect of temperature and strain rate on plasticity of the hydrogen-free (dashed line) and hydrogen-charged, 2 cm^3 H_2 per 100 g metal, (solid lines) alloy FeCr05. According to Popov [7]

ture-dependent internal friction (TDIF); see, *e.g.*, hydrogen-caused Snoek-like relaxation in hydrogen-charged β-titanium alloy (Fig. 14) and austenitic steel Cr25Ni25 (Fig. 15).

The strain-induced hops of interstitial atoms constitute a mechanism of Snoek-like relaxation. The frequency shifts of relaxation peaks, as presented in the inset, make it possible to obtain the values of diffusion enthalpy. Comparing hydrogen Snoek-like peak temperatures in titanium and austenitic steel, one can see how different hydrogen diffusivity is in these materials.

It is clear that binding between hydrogen atoms and dislocations is the highest in b.c.c.-Fe. It is much smaller in austenitic steels, increased by chromium and manganese, but decreased by nickel and copper. The smallest enthalpy of hydrogen–dislocation binding occurs in pure nickel, the nickel alloy Inconel 718 and, particularly, in β-titanium alloy.

Some correlation occurs between diffusion enthalpy ΔH_d, the enthalpy ΔH_b of their binding to dislocations and condensation temperature T_c. Manganese and chromium in austenitic steels retard hydrogen diffusion, enhance hydrogen–dislocation binding and increase the temperature of hydrogen condensation at dislocations. Compared to austenitic steels, the nickel alloy Inconel 718 is characterized by faster migration of hydrogen atoms and smaller hydrogen–dislocation binding, which corresponds to a decrease in the condensation temperature. The extremely low values of ΔH_b and ΔH_d in the b.c.c. titanium alloy represent a particular case of high hydrogen-atoms' diffusivity and their weak binding with dislocations. Accordingly, the condensation temperature is too low to be measured in the current experiment. A special case is hydrogen in b.c.c. iron,

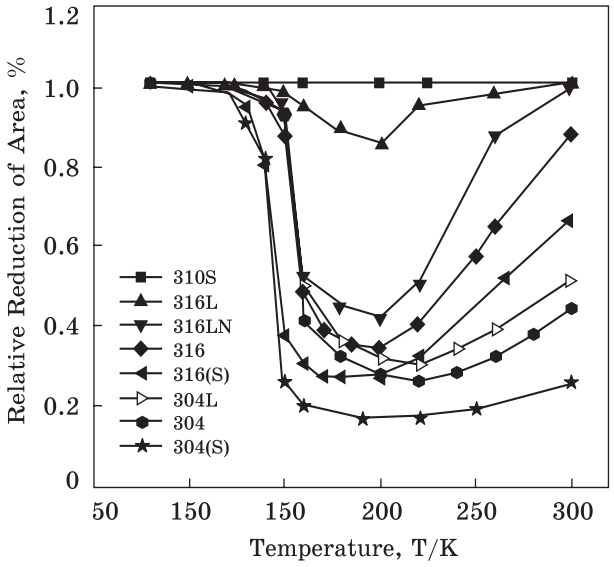

Fig. 18. Effect of temperature on relative reduction of area of stainless steels in 1.1 MPa hydrogen and helium at low temperatures. 304 solution-annealed 304 stainless steel, 304(S) sensitized 304 stainless steel, 316 solution-annealed 316 stainless steel and 316(S) sensitized 316 stainless steel. Redrawn from Fukuyama *et al.* [114]

where hydrogen–dislocation binding is rather strong and hydrogen diffusivity is extremely high.

Thus, the enthalpies of hydrogen diffusion and hydrogen binding to dislocations control the hydrogen condensation temperature at dislocations. Considering this, let us analyse available data about the temperature range of hydrogen embrittlement (see Figs. 16–18).

Hydrogen atoms in pure nickel at temperatures of 77 K and up to 150 K are 'frozen' and are simply point obstacles for moving dislocations. Ductility even slightly increases because of the hydrogen-caused softening of the crystal lattice. As follows from Fig. 15, hydrogen embrittlement starts within 120 to 150 K. This temperature is close to that of hydrogen condensation at dislocations for Inconel 718 (see Table 5) and reaches its maximum in the temperature range of 150 to 225 K. The highest brittleness occurs at nearly $\gg$250 K, which is conceivably relates to compatible rates of hydrogen diffusion and dislocation slip. The increase in the strain rate by one order of magnitude reduces the loss of plasticity, slightly shifts it to higher temperatures and assists restoration of plasticity as temperature increases, which is obviously caused by the weakening of hydrogen–dislocation binding.

Unfortunately, there are no data on T_c for iron doped with chromium that makes it impossible to interpret the start temperature of hydrogen embrittlement as $\gg$165 K (see Fig. 17).

Such analysis could be particularly useful because of the opposite hydrogen effects on the enthalpies of hydrogen diffusion and hydrogen–dislocation binding.

The experimental data obtained by Fukuyama *et al.* [114] for the temperature range of hydrogen embrittlement in stainless austenitic steels (see Fig. 18) are of interest.

Our experimental data for steels Cr15Ni25 and Cr25Ni25 obtained using melting in a vacuum with pure chemical components, as presented in Table 4, can be only roughly analysed in the comparison with those for industrial steels 310, 316 and 304. The hydrogen condensation temperatures in steels Cr15Ni25 and Cr25Ni25 are 175 and 190 K, and their hydrogen embrittlement is expected to start at higher temperatures in comparison with industrial steels.

Steel AISI 310S is shown to be stable against hydrogen, although the H condensation temperature of steel Cr25Ni25 similar in its chemical composition suggests the occurrence of hydrogen embrittlement if the short-range atomic decomposition occurs.

A huge difference in the hydrogen-caused loss of ductility in steels 316 and 316L demonstrates the strong dependence of hydrogen-caused damage to ductility on the content of unintentionally introduced elements like carbon.

The comparison of HE in steels 316L and 316LN shows nitrogen having a negative effect on resistance to HE caused by the nitrogen-increased concentration of free electrons (see Refs. [99] and [115]) and combined with nitro-gen-induced short-range atomic ordering in austenitic steels (see Ref. [101]).

The increase in hydrogen embrittlement due to sensitization treatment in steels 316(S) and 304(S) points to the significant role played by short-range atomic decomposition of solid solutions in hydrogen embrittlement. Martensitic transformation in steel 304 at low temperatures also worsens its resistance to HE.

4.3. Hydrogen-Increased Plasticity of Metallic Alloys

The following experimental data confirm the intrinsic property of hydrogen as an element increasing the plasticity of metallic alloys.

4.3.1. Hydrogen as a Temporary Alloying Element

Zwicker and Schleicher [116] were the first to detect, by chance, that hydrogen improves the hot deformability of cast titanium alloys. A Ti–8% Al ingot containing 0.061% H has been successfully deformed at 950 °C using a single deformation by 65%, whereas a hydrogen-free billet was completely destroyed by this deformation. A feature of their experiment was the hydrogen charging of the ingot, not the semi-finished product. A reason for that was not provided.

In fact, this unorthodox result confirms the dominant role of short-range atomic order in the localization of plastic deformation in metallic

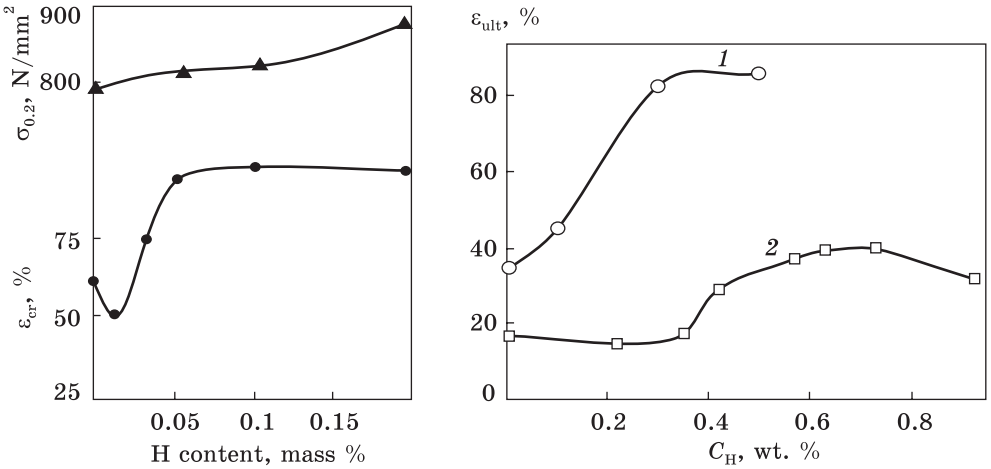

Fig. 19. Hydrogen effect on yield strength $\sigma_{0.2}$ and critical upsetting deformation degree ε_{cr} of quenched alloy VT30 at RT before the appearance of the first crack. Redrawn from Kolachev [123]

Fig. 20. Hydrogen effect on the ultimate plasticity of VT 221 (*1*) and Ti–10V–2Fe–3Al (*2*) alloys during cold deformation. Redrawn from Nosov *et al.* [125]

alloys (see Sec. 3). Inherited from the melt, the nearly random atomic distribution in the ingot is close to that in ideal metallic solutions, which prevents the hydrogen-enhanced localization of dislocation slip. The plastic deformation of ingots at high temperatures accelerates the diffusion of metallic atoms and assists the short-range atomic decomposition of solid solutions resulting in non-homogeneous hydrogen distribution and the consequent localization of plastic deformation.

There were no publications on this topic for a long time after the experiments by Zwicker and Schleicher. The first published studies belong to Kolachev *et al.* [117], who deformed Ti–Al alloys doped with 0.1% of hydrogen after melting. The critical deformation not leading to cracking during hot compression at 950 °C was equal to 25%. Along with superior deformability, significantly decreased stress, from 30 kg/mm^2 down to 6 kg/mm^2, was sufficient for deformation.

Possible mechanisms proposed for a positive hydrogen effect in Ti–Al alloys included the hydrogen-caused stabilization of the soft b.c.c. β-phase at lower temperatures, prevention of precipitation in the brittle intermetallic α_2-phase Ti_3Al, the enhanced diffusion of metallic atoms in the β phase compared with that in the α phase, and the realization of new systems of dislocation slip (see Refs. [118–120]).

A number of experimental data obtained in subsequent studies of high-temperature hydrogen-enhanced plasticity in titanium alloys were reviewed in details by Eliezer *et al.* [121], Froes *et al.* [122, 123], *etc*.

Kolachev *et al.* [124] were also the first to demonstrate a favourable hydrogen effect on the plasticity of β-alloy VT15 (Ti–11Cr–7Mo) and transition alloy VT30 (Ti–11Mo–6Zr–4.5Sn) at ambient temperatures (see Fig. 19). At hydrogen content higher than 1 mas.%, cylindrical samples of 10 mm in diameter and 15 mm in length were deformed close to 100% during upsetting tests.

Later, Nosov *et al.* [125, 126] demonstrated high deformability at ambient temperature of β-alloys VT22 (Ti–5Al–5Mo–1Cr–1Fe), VT22I (Ti–3Al–5Mo–1Cr–1Fe) and the alloy Ti–10V–2Fe–3Al (see Fig. 20).

Remarkably, these effects follow directly from the hydrogen effect on the electron structure and properties of dislocations. Hydrogen embrittlement is absent in β-titanium alloys due to the combined action of extremely small values of hydrogen diffusion and hydrogen binding with dislocations enthalpies, which shifts the temperature range of its possible realization to temperatures close to that of liquid nitrogen. For this reason, at ambient temperatures, the hydrogen-increased concentration of free electrons is realized only in the softening of the crystal lattice without any local effects at dislocations.

4.3.2. Hydrogen in Austenitic Steels

A peculiar phenomenon of hydrogen-increased fatigue life in 304 and 316 austenitic steels was observed by Murakami *et al.* [127]. As follows from Fig. 21, the hydrogen-accelerated growth of a fatigue crack in steel 304 containing 23.9 ppm of hydrogen is replaced by its slowdown with a further increase in hydrogen content.

The authors interpreted this result in terms of supposed hydrogen-caused softening/hardening, claiming that dislocations are pinned by hydrogen atoms located at the dislocations. Released from pinning by hydrogen at its core, the dislocation acquires higher mobility. However, as hydrogen content increases, the plastic zone at a crack tip is blocked by surrounding material with a higher flow stress. This phenomenon retards fatigue crack growth rate.

Quite a different explanation has been given by Kirchheim [128] based on his defactant theory for the formation and motion of kinks under the effect of mobile solute interstitial atoms. According to Kirchheim, time τ_g for double kink generation, and time τ_m needed to move the kinks to the ends of a dislocation segment, control dislocation slip. Solute atoms segregated at dislocations decrease τ_g. If $\tau_m < \tau_g$, the strain rate increases, *i.e.*, softening occurs. With increasing contents of solutes, they enhance the dragging force on the moving kinks and τ_m increases, which results in $\tau_m > \tau_g$. In the case of austenitic steels supersaturated by hydrogen atoms, their drag on the kinks dominates over the hydrogen-caused enhancement of kink formation leading to decreased strain rate, *i.e.*, to hardening.

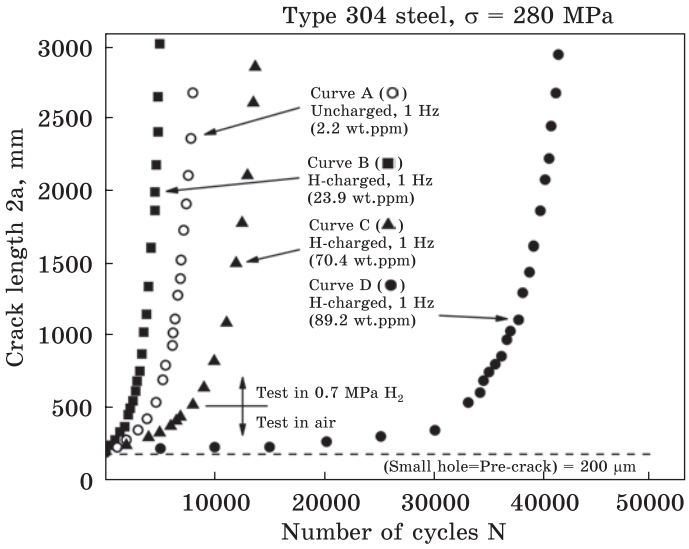

Fig. 21. Effect of hydrogen content on fatigue crack growth. Adopted from Murakami *et al.* [127]

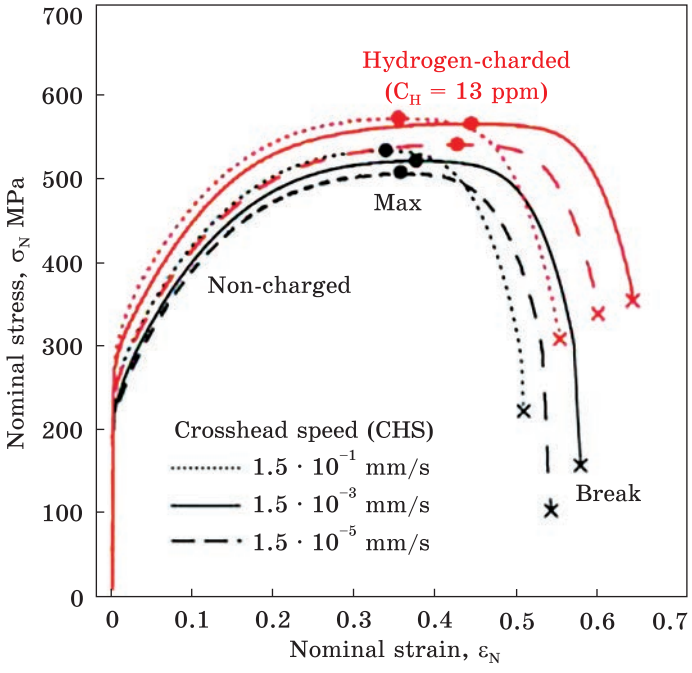

Fig. 22. Stress–strain curves of a type 310S stainless steel doped with hydrogen. Tested in air with strain rates of $5.0 \cdot 10^{-5}$, $5.0 \cdot 10^{-3}$ and $5.0 \cdot 10^{-1}$ s^{-1}. Redrawn from Ogava *et al.* [141]

However, the Peierls relief is rather shallow in the f.c.c. crystal lattice of austenitic steels and kinks are extremely broadened so that plastic deformation can be hardly described in terms of formation and movement of the kinks. In particular for this reason, the Snoek–Köster relaxation caused by the formation of kinks and their interaction with dislocations

occurs in metals and alloys with the b.c.c. crystal lattice and is absent in f.c.c. metals and austenitic steels. The only exception among the f.c.c. metals is a pure Ni, where stacking fault energy is close to that in Fe, dislocation kinks are narrow and, consequently, H causes Snoek–Köster relaxation peak (see Ref. [129]). According to Seeger's theory for the yield stress in the f.c.c. metals [130, 131], the movement of dislocations under applied stress is controlled by their intersections, not by kink formation and motion. This theory was confirmed for austenitic steels by Obst and Nyilas [132], Nyilas *et al.* [133], and Gavriljuk *et al.* [134], as well as for the CuNiMn and AlMgMn alloys and copper by Obst [135].

More reliable is the interpretation of hydrogen-prolonged fatigue life in austenitic steels based on the specific character of plastic deformation during fatigue tests (see Ref. [136]). Margolin *et al.* [137] studied earlier fatigue crack initiation in compression-tension tests depending on the character of dislocation slip. They were first to detect that reversed deformation during fatigue tests produces folds accompanying the wavy slip in Cu and Al, whereas in the case of Cu–7.5Al alloy, these folds are absent and characterized by a planar slip mode. As a result, the reversible gliding of dislocations on the same slip planes should be localized in the slip bands accompanied by the annihilation of dislocations with opposite signs and causing increased fatigue life.

In fact, the localization of reversible plastic deformation in the slip bands is a consequence of a significant deviation in the atomic distribution from that of ideal solid solutions, namely short-range atomic order. For example, Epperson *et al.* [138] observed a prevailing Cu–Al neighbourhood and the absence of the Al–Al nearest neighbour pairs in CuAl alloys.

It is worth noting that, similarly to the observations by Murakami *et al.* [127] for hydrogen, Tobler and Reed [139] found that nitrogen decreased the fatigue crack propagation rate in the AISI 304 type steel Cr18Ni10, if the nitrogen content increased from 0.039 to 0.240 wt.%. This result was confirmed by Taillard and Foct [140], who carried out a thorough analysis of dislocation substructure in the AISI 316 steel alloyed with 0.08 or 0.25% of N in comparison with the fatigue tests.

The data presented make it possible to conclude that the hydrogen effect against hydrogen embrittlement, as found by Murakami *et al.*, is identical to that caused by nitrogen in austenitic steels. Based on the similarity of hydrogen and nitrogen effects on their electron structure and dislocation properties, and taking into account the occurrence of short-range atomic order in both cases, one can conclude that the Murakami effect represents a unique combination of specific tension–compression plastic deformation localized within the dislocation bands thanks to a short-range atomic order and the softening of the crystal lattice by the increased concentration of free electrons, thereby, assisting reversible dislocation slip.

It would not go amiss to mention that hydrogen increases plasticity in austenitic steel AISI type 310 containing 24 mas.% of Cr and 19.4 mas.% of Ni (see Ref. [141] and Fig. 22).

Plasticity characterized by relative elongation, as well as yield and ultimate strengths were shown to be increased with increasing hydrogen content. The non-monotonous dependence of plasticity in steel containing the remaining 5 ppm and that charged with 133 ppm of hydrogen on the increasing strain rate is remarkable. In both cases, relative elongation is enhanced with an increase in strain rate from $5.0 \cdot 10^{-7}$ to $5.0 \cdot 10^{-3}$ s^{-1} and decreases at the higher strain rate of $5.0 \cdot 10^{-3}$ s^{-1}.

The improved plasticity is obviously caused by the hydrogen-decreased line tension of dislocations encased in the hydrogen atmospheres, where the concentration of free electrons is locally increased. At sufficiently high strain rates, dislocations are released from hydrogen atmospheres, thereby decreasing their velocity.

5. Summary

A mechanism of hydrogen embrittlement of metallic alloys has been described in terms of hydrogen effect on the electron structure. Hydrogen dissolution changes the distribution of valence electrons across their energy levels, increasing the density of electron states at the Fermi level. Correspondingly, the concentration of free electrons increases, which softens the crystal structure and should increase plasticity, owing to a decrease in the line tension of dislocations and a corresponding increase in their velocity.

However, this positive hydrogen effect can lead to pseudo-brittle fracture if plastic deformation is localized. A deviation from the random distribution of solute atoms, namely, short-range atomic order of both types, namely, ordering and decomposition, in solid solutions is shown to be a precondition for hydrogen embrittlement. In pure metals, localized plasticity can also be caused by hydrogen-induced superabundant vacancies concentrated within the actual slip planes in hydrogen atmospheres around moving dislocations. Hydrogen segregation at the grain boundaries leading to their saturation with vacancies is thought to be the main reason for intercrystalline fracture in metals.

Using strain-dependent internal friction, hydrogen-enhanced dislocation mobility has been confirmed, and enthalpies of hydrogen–dislocation binding in austenitic steels, nickel and titanium alloys, have been obtained. As a result, the temperatures of hydrogen condensation at dislocations have been determined, above which moving dislocations are accompanied by hydrogen-atoms' atmospheres. It is concluded that, along with the data on hydrogen diffusion enthalpy obtained from measurements of temperature-dependent internal friction, these values control the temperature range of hydrogen embrittlement, if localization of plastic deformation occurs. The condensation temperature of hydrogen at dislocations in

the solution-treated nickel alloy Inconel 718 is consistent with the available data on hydrogen embrittlement in pure nickel. Combined measurements of H-condensation temperatures and mechanical tests on industrial austenitic steels are desirable for estimation that is more precise.

A positive hydrogen effect on the fatigue life of austenitic steels, the hydrogen-enhanced plasticity of a β-titanium alloy and type 310S stainless steel, has been analysed in terms of hydrogen–dislocation interaction.

Acknowledgement. The research is performed within the framework of the State Budget Project No. 044/23 (0123U100539) of G.V. Kurdyumov Institute for Metal Physics of the National Academy of Sciences of Ukraine.

REFERENCES

1. W.H. Johnson, On some remarkable changes produced in iron and steel by the action of hydrogen and acid, *Proc. Royal Society of London*, **23**, No. 158: 168 (1875). Republished in *Hydrogen Damage* (Metals Park, OH: ASM: 1977).
2. J.P. Hirth and H.H. Johnson, Hydrogen problems in energy related technology, *Corrosion*, **32**, No. 1: 3 (1976); https://doi.org/10.5006/0010-9312-32.1.3
3. M.R. Louthan Jr. *Hydrogen in Metals* (Eds. I.M. Bernstein and A.W. Thompson) (Metals Park, OH: ASM: 1974), pp. 53–78.
4. I.M. Bernstein, R. Garber, and G.M. Presouyre, Effect of dissolved hydrogen on mechanical behavior of metals, *Effect of Hydrogen on Behavior of Materials* (Eds. A.W. Thompson and I.M. Bernstein) (New York: TMS-AIME: 1975), pp. 37–58.
5. P. Bastien and P. Azou, Influence de l'écrouissage sur le frottement intérieur du fer et del'acier, chargés ou non en hydrogene, *C. R. Acad. Sci. Paris*, **232**: 1845–1848 (1951) (in French).
6. T. Boniszewski and G.C. Smith, The influence of hydrogen on the plastic deformation ductility and fracture of nickel in tension, *Acta Metall.*, **11**, No. 3: 165–178 (1963); https://doi.org/10.1016/0001-6160(63)90209-8
7. K.V. Popov, Dynamical strain aging of metals and hydrogen-type brittleness (Novosibirsk: Nauka, Siberia branch: 1969), 98 pp. (in Russian).
8. R.M. Gabidullin, B.A. Kolachev, and P.D. Drozdov, Estimation of conditions for manifestation of reversible hydrogen brittleness of metals, *Problems of Strength*, No. 12: 36–40 (1971) (in Russian).
9. L. Fournier, D. Delafosse, and T. Magnin, Cathodic hydrogen embrittlement in alloy 718, *Mat. Sci. Eng. A*, **269**, Nos. 1–2: 111–119 (1999); https://doi.org/10.1016/s0921-5093(99)00167-7
10. C. Zapfe, Discussion of metal arc welding of steels by S.A. Herres, *Trans. ASM*, No. 39: 191–192 (1947).
11. F. Garofalo, Y.T. Chou, and V. Ambegaokar, Effect of hydrogen on stability of micro cracks in iron and steel, *Acta Metall.*, **8**, No. 8: 504–512 (1960); https://doi.org/10.1016/0001-6160(60)90103-6
12. B.A. Bilby and J. Hewitt, Hydrogen in steel — the stability of micro-cracks, *Acta Metall.*, **10**, No. 6: 587–600 (1962); https://doi.org/10.1016/0001-6160(62)90048-2
13. N.J. Petch, Delayed fracture of metals under static load, *Nature*, **169**: 842–843 (1952); https://doi.org/10.1038/169842a0

14. N.J. Petch, The lowering of fracture-stress due to surface adsorption, *Phil. Mag.*, **1**, No. 4: 331–337 (1956); https://doi.org/10.1080/14786435608238106
15. A.R. Troiano, The role of hydrogen and other interstitials in the mechanical behavior of metals, *Trans. ASM*, **52**, 54–80 (1960). Republished: A.R. Troiano, *Metallogr. Microstruct. Anal.*, **5**: 557–569 (2016); https://doi.org/10.1007/s13632-016-0319-4
16. E.A. Steigerwald, F.W. Schaller, and A.R. Troiano, The role of stresses in hydrogen induced delayed failure, *TMS-AIME*, **218**, No. 5: 832–841 (1960).
17. R.A. Oriani, A mechanistic theory of hydrogen embrittlement of steels, *Berichte Bunsen Gesellschaft fьr Physik Chem*, **76**, No. 8: 848–857 (1972); https://doi.org/10.1002/bbpc.19720760864
18. R.A. Oriani and P.H. Josephic, Testing of the decohesion theory of hydrogen-induced crack propagation, *Scripta Metall.*, **6**, No. 8: 681–688 (1972); https://doi.org/10.1016/0036-9748(72)90126-3
19. R.A. Oriani and P.H. Josephic, Equilibrium aspects of hydrogen-induced cracking of steels, *Acta Metall*, **22**, No. 9: 1065–1074 (1974); https://doi.org/10.1016/0001-6160(74)90061-3
20. R.A. Oriani and P.H. Josephic, Equilibrium and kinetic studies of the hydrogen-assisted cracking of steel, *Acta Metall.*, **25**, No. 9: 979–988 (1977); https://doi.org/10.1016/0001-6160(77)90126-2
21. S.P. Lynch, Environmentally assisted cracking: Overview of evidence for an adsorption-induced localised-slip process, *Acta Metall.*, **36**, No. 10: 2639–2661 (1988); https://doi.org/10.1016/0001-6160(88)90113-7
22. S.P. Lynch, Towards understanding mechanisms and kinetics of environmentally assisted cracking, *Environment-Induced Cracking of Materials* (Eds. S.A. Shipilov, R.H. Jones, J.-M. Olive, and R.B. Rebak) (Elsevier: 2008), pp. 167–177.
23. S. Lynch, Hydrogen embrittlement phenomena and mechanisms, *Corros Rev.*, **30**, Nos. 3–4: 105–123 (2012); https://doi.org/10.1515/corrrev-2012-0502
24. M. Nagumo, Function of hydrogen in embrittlement of high-strength steels, *ISIJ Intern.*, **41**, No. 6: 590–598 (2001); https://doi.org/10.2355/isijinternational.41.590
25. M. Nagumo, Hydrogen related failure of steels — a new aspect, *Mat. Sci. Technol.*, **20**, No. 8: 940–950 (2004); https://doi.org/10.1179/026708304225019687
26. M. Nagumo and K. Takai, The predominant role of strain-induced vacancies in hydrogen embrittlement of steels: Overview, *Acta Mater.*, **165**: 722–733 (2019); https://doi.org/10.1016/j.actamat.2018.12.013
27. J. Song, M. Soar, and W.A. Curtin, Testing continuum concepts for hydrogen embrittlement in metals using atomistics, *Model. Simul. Mater. Sci.*, **18**: 045003 (2010); https://doi.org/10.1088/0965-0393/18/4/045003
28. J. Song and W.A. Curtin, Atomic mechanism and prediction of hydrogen embrittlement in iron, *Nature Mat.*, **12**, No. 2: 145–151 (2012); https://doi.org/10.1038/nmat3479
29. A. Tehranchi, X. Zhou, and W.A. Curtin, A decohesion pathway for hydrogen embrittlement in nickel: mechanism and quantitative prediction, *Acta Mater.*, **185**, No. 15: 98–109 (2020); https://doi.org/10.1016/j.actamat.2019.11.062
30. H.K. Birnbaum and P. Sofronis, Hydrogen-enhanced localized plasticity — a mechanism for hydrogen-related fracture, *Mat. Sci. Eng. A*, **176**, Nos. 1–2: 191–202

(1994);
https://doi.org/10.1016/0921-5093(94)90975-x
31. I.M. Robertson, The effect of hydrogen on dislocation dynamics, *Eng. Fract. Mech.*, **64**, No. 5: 649–673 (1999);
https://doi.org/10.1016/s0013-7944(99)00094-6
32. P. Sofronis and I.M. Robertson, Transmission electron microscopy observations and micromechanical/continuum models for the effect of hydrogen on the mechanical behaviour of metals, *Phil. Mag. A*, **82**, Nos. 17–18: 3405–3413 (2002);
https://doi.org/10.1080/01418610208240451
33. I.M. Robertson, P. Sofronis, A. Nagao, M.L. Martin, S. Wang, D.V. Gross, and K.E. Nygren, Hydrogen embrittlement understood, *Metall. Mater. Trans. A*, **46**, No. 3: 1085–1103 (2015);
https://doi.org/10.1007/s11663-015-0325-y
34. A. Nagao, M. Dadfarnia, P. Sofronis, and I. Robertson, *Hydrogen Embrittlement: Mechanisms. Encyclopedia of Iron, Steel, and Their Alloys* (Taylor & Francis: 2015), pp. 1768–1784;
https://doi.org/10.1081/E-EISA-120049717
35. A. Nagao, M. Dadfarnia, B.P. Somerday, P. Sofronis, and R.O. Ritchie, Hydrogen-enhanced-plasticity mediated decohesion for hydrogen-induced intergranular and "quasi-cleavage" fracture of lath martensitic steels, *J. Mech. Phys. Sol.*, **112**: 403–430 (2018);
https://doi.org/10.1016/j.jmps.2017.12.016
36. M.L. Martin, M. Dadfarnia, A. Nagao, S. Wang, and P. Sofronis, Enumeration of the hydrogen-enhanced localized plasticity mechanism for hydrogen embrittlement in structural materials, *Acta Mater.*, **165**: 734–750 (2019);
https://doi.org/10.1016/j.actamat.2018.12.014
37. P. Sofronis and H.K. Birnbaum, Mechanics of the hydrogen–dislocation–impurity interactions. — I. Increasing shear modulus, *J. Mech. Phys. Sol.*, **43**, No. 1: 49–90 (1995);
https://doi.org/10.1016/0022-5096(94)00056-b
38. P.J. Ferreira, I.M. Robertson, and H.K. Birnbaum, Hydrogen effects on the interaction between dislocations, *Acta Mater.*, **46**, No. 5: 1749–1757 (1998);
https://doi.org/10.1016/S1359-6454(97)00349-2
39. P.J. Ferreira, I.M. Robertson, and H.K. Birnbaum, Hydrogen effects on the character of dislocations in high-purity aluminium, *Acta Mater.*, **47**, No. 10 2991–2998 (1999);
https://doi.org/10.1016/s1359-6454(99)00156-1
40. D.G. Ulmer and C.J. Altstetter, Hydrogen-induced strain localization and failure of austenitic stainless steels at high hydrogen concentrations, *Acta Metall. Mater.*, **39**, No. 6: 1237–1248 (1991);
https://doi.org/10.1016/0956-7151(91)90211-I
41. M.-J. Lji, X.-F. Chen, Y. Katz, and W.W. Gerberich, Dislocation modeling and acoustic emission observation of alternating ductile/brittle events in Fe-3wt%Si crystals, *Acta Metall. Mater.*, **38**, No. 12: 2435–2453 (1990);
https://doi.org/10.1016/0956-7151(90)90255-f
42. W.W. Gerberich, R.A. Oriani, M.-J. Lji, X. Chen, and T. Foecke, The necessity of both plasticity and brittleness in the fracture thresholds of iron, *Phil. Mag. A*, **63**, No. 2: 363–376 (1991);
https://doi.org/10.1080/01418619108204854
43. W.W. Gerberich, D.D. Stauffer, and P. Sofronis, A coexistent view of hydrogen effects on mechanical behaviour of crystals: HELP and HEDE. Effect of Hydrogen

on Materials (Eds. B. Somerday, P. Sofronis, and R. Jones), *Proc. of Int. Hydrogen Conf.* (ASM: 2009), pp. 38–45.
44. M.B. Djukic, V.S. Zeravcic, G.M. Bakic, A. Sedmak, and B. Rajicic, Hydrogen damage of steels: A case study and hydrogen embrittlement model, *Eng. Failure Anal.*, **58**: 485–498 (2015); https://doi.org/10.1016/j.engfailanal.2015.05.017
45. M.B. Djukic, G.M. Bakic, V.S. Zeravcic, A. Sedmak, B. Rajicic, Hydrogen Embrittlement of Industrial Components: Prediction, Prevention, and Models, *Corrosion*, **72**, No. 7: 943–961 (2016); https://doi.org/10.5006/1958
46. M.B. Djukic, G.M. Bakic, V. Sijacki Zeravcic, A. Sedmak, and B. Rajicic, The synergistic action and interplay of hydrogen embrittlement mechanisms in steels and iron: Localized plasticity and decohesion, *Eng. Fract. Mech.*, **216**: 106528 (2019); https://doi.org/10.1016/j.engfracmech. 2019.106528
47. A. Nagao, C.D. Smith, M. Dadfarnia, P. Sofronis, and I.M. Robertson, The role of hydrogen in hydrogen embrittlement fracture of lath martensitic steel, *Acta Mater.*, **60**, Nos. 13–14: 5182–5189 (2012); https://doi.org/10.1016/j.actamat.2012.06.040
48. A. Nagao, M. Dadfarnia, P. Sofronis, and I. Robertson, *Hydrogen Embrittlement: Mechanisms. Encyclopedia of Iron, Steel, and Their Alloys* (Taylor & Francis: 2016), pp. 1768–1784; https://doi.org/10.1081/E-EISA-120049717
49. A. Nagao, M. Dadfarnia, B.P. Somerday, P. Sofronis, and R.O. Ritchie, Hydrogen-enhanced-plasticity mediated decohesion for hydrogen-induced intergranular and "quasi-cleavage" fracture of lath martensitic steels, *J. Mech. Phys. Sol.*, **112**: 403–430 (2018); https://doi.org/10.1016/j.jmps.2017.12.016
50. K.M. Bertch, S. Wang, A. Nagao, and I.M. Robertson, Hydrogen-induced compatibility constraints across grain boundary drive intergranular failure of Ni, *Mat. Sci. Eng. A*, **760**: 58–67 (2019); https://doi.org/10.1016/j.msea.2019.05.36
51. K.E. Nygren, A. Nagao, S. Wang, P. Sofronis, and I.M. Robertson, Influence of internal hydrogen content on the evolved microstructure beneath fatigue striations in 316L austenitic stainless steel, *Acta Mater.*, **213**: 116957 (2021); https://doi.org/10.1016/j.actamat.2021.116957
52. Z.D. Harris, S.K. Lawrence, D.L. Medlin, G. Guetard, J.T. Burns, and B.P. Somerday, Elucidating the contribution of mobile hydrogen-deformation interactions to hydrogen-induced intergranular cracking in polycrystalline nickel, *Acta Mater.*, **158**: 180–192 (2018); https://doi.org/10.1016/j.actamat.2018.07.043
53. B.D. Shanina, V.G. Gavriljuk, S.P. Kolesnik, and V.N. Shivanyuk, Paramagnetic resonance in hydrogen-charged austenitic steel, *J. Phys. D: Appl. Phys.*, **32**, No. 3: 298–304 (1999); https://doi.org/10.1088/0022-3727/32/3/018
54. S.M. Teus, V.N. Shyvanyuk, B.D. Shanina, and V.G. Gavriljuk, Effect of hydrogen on electronic structure of fcc iron in relation to hydrogen embrittlement of austenitic steels, *Phys. Stat. Sol. A*, **204**, No. 12: 4249–4258 (2007); https://doi.org/10.1002/pssa.200723249
55. V.G. Gavriljuk, B.D. Shanina, V.N. Shyvanyuk, and S.M. Teus, Electronic effect on hydrogen brittleness of austenitic steels, *J. Appl. Phys.*, **108**: 083723 (2010); https://doi.org/10.1063/1.3499610

56. S.M. Teus and V.G. Gavriljuk, Electron structure and thermodynamics of solid solutions in Ni–H system, *Mat. Sci. & Eng. Int. J.*, **2**, No. 4: 101–109 (2018); https://doi.org/10.15406/mseij.2018.02.00042
57. V.G. Gavriljuk, V.M. Shyvaniuk, and S.M. Teus, *Hydrogen in Engineering Metallic Materials* (Springer: 2022); https://doi.org/10.1007/978-3-030-98550-9
58. H.K. Birnbaum, I.M. Robertson, P. Sofronis, and D. Teter, Mechanisms of hydrogen related fracture — A review, *Second Int. Conf. 'Corrosion, Deformation Interactions CDI'96' (Nice, France)* (Ed. T. Magnin) (Great Britain: The Institute of Materials: 1997), pp. 172–195.
59. P. Sofronis, Y. Liang, and N. Aravas, Hydrogen induced shear localization of the plastic flow in metals and alloys, *Eur. J. Mech. A/Solids*, **20**, No. 6: 857–872 (2001); https://doi.org/10.1016/S0997-7538(01)01179-2
60. I.M. Robertson, H.K. Birnbaum, P. Sofronis, *Hydrogen Effects on Plasticity. Dislocations in Solids* (Eds. J.P. Hirth and L. Kubin) (Elsevier: 2009), Ch. 91, pp. 249–293.
61. C. Hwang and I.M. Bernstein, The effect of strain on hydrogen-induced dislocation morphologies in single crystal iron, *Acta Metall.*, **34**, No. 6: 1011–1020 (1986); https://doi.org/10.1016/0001-6160(86)90210-5
62. T.D. Le and I.M. Bernstein, Effects of hydrogen on dislocation morphology in spheroidized steel, *Acta Metall. Mater.*, **39**, No. 3: 363–372 (1991); https://doi.org/1010.1016/0956-7151(91)90315-r
63. W.A. McInteer, A.W. Thompson, and I.M. Bernstein, The effect of hydrogen on the slip character of nickel, *Acta Metall.*, **28**, No. 7: 887–894 (1980); https://doi.org/10.1016/0001-6160(80)90105
64. S. Wang, A. Nagao, K. Edalati, Z. Horita, and I.M. Robertson, Influence of hydrogen on dislocation self-organization in Ni, *Acta Mater.*, **135**: 96–102 (2017); https://doi.org/10.1016/j.actamat.2017.05.073
65. W.A. Tayon, K.E. Nygren, R.E. Crooks, and D.C. Pagan, *In-situ* study of planar slip in a commercial aluminum–lithium alloy using high energy x-ray diffraction microscopy, *Acta Mater.*, **173**: 231–241 (2019); https://doi.org/10.1016/j.actamat.2019.04.030
66. M. Furukawa, Y. Miura, and M. Nemoto, Strengthening mechanisms in Al–Li alloys containing coherent ordered phases, *Trans. Jpn. Inst. Metals*, **26**, No. 4: 230–235 (1985); https://doi.org/10.2320/matertrans1960.26.230
67. H. Zhao, P. Chakraborty, P. Ponge, T. Hickel, B. Sun, C.-H. Wu, B. Gault, and D. Raabe, Hydrogen trapping and embrittlement in high-strength Al alloys, *Nature*, **602**, No. 7897: 437–441 (2022); https://doi.org/10.1038/s41586-021-04343-z
68. P.L. Gruzin, Yu.V. Kornev, and G.V. Kurdyumov, Hydrogen effect on selfdiffusion of the iron, *Dokl. Akad. Nauk SSSR*, **LXXX**, No. 1: 49–51 (1951) (in Russian).
69. R.B. McLellan, The thermodynamics of interstitial–vacancy interactions in solid solutions, *J. Phys. Chem. Solids*, **49**, No. 10: 1213–1217 (1988); https://doi.org/10.1016/0022-3697(88)90178-3
70. A.A. Smirnov, Theory of vacancies at crystal lattice sites in interstitial alloys, *Dokl. Akad. Nauk Ukr. SSR*, No. 7: 66–71 (1991) (in Russian).
71. N.Z. Carr and R.B. McLellan, The thermodynamic and kinetic behavior of metal–vacancy–hydrogen systems, *Acta Mater.*, **52**, No. 11: 3273–3293 (2004); https://doi.org/10.1016/j.actamat.2004.03.024

72. Y. Fukai and N. Okuma, Evidence of copious vacancy formation in Ni and Pd under a high hydrogen pressure, *Jpn. J. Appl. Phys.*, **32**, No. 9A: L1256–L1259 (1993);
https://doi.org/10.1143/JJAP.32.L1256
73. V.G. Gavriljuk, V.N. Bugaev, Yu.N. Petrov, A.V. Tarasenko, and B.Z. Yanchitski, Hydrogen-induced equilibrium vacancies in fcc iron base alloys, *Scr. Mater.*, **34**, No. 6: 903–907 (1996);
https://doi.org/10.1016/1359-6462(95)00580-3
74. Y. Takeyama and T. Ohno. Stability and clusterization of hydrogen–vacancy complexes in α-Fe, *Phys. Rev. B*, **67**, No. 17: 174105 (2003);
https://doi.org/10.1103/PhysRevB.67.174105
75. W.A. Counts, C. Wolverton, and R. Gibala, First-principles energetic of hydrogen traps in α-Fe: Point defects, *Acta Mater.*, **58**, No. 14: 4730–4741 (2010);
https://doi.org/10.1016/j.actamat.2010.05.010
76. R. Nazarov, T. Hickel, and J. Neugebauer, First-principles study of the thermodynamics of hydrogen–vacancy interaction in fcc iron, *Phys. Rev. B*, **82**, No. 22: 224104 (2010);
https://doi.org/10.1103/PhysRevB.82.224104
77. G. Lu and E. Kaxiras, Hydrogen embrittlement of aluminum: The crucial role of vacancies, *Phys. Rev. Lett.*, **94**, No. 15: 155501 (2005);
https://doi.org/10.1103/PhysRevLett.94.155501
78. H.K. Birnbaum, C. Buckley, F. Zeides, E. Sirois, P. Rozenak, S. Spooner, and J.S. Lin, Hydrogen in aluminium, *J. Alloys Compd.*, **253–254**: 260–264 (1997);
https://doi.org/10.1016/S0925-8388(96)02968-4
79. D. Teirlinck, F. Zok, J.D. Embury, and M.F. Ashby, Fracture mechanism maps in stress space, *Acta Metall.*, **36**, No. 5: 1213–1228 (1988);
https://doi.org/10.1016/0001-6160(88)90274-X
80. W. Charnock and J. Nutting, The effect of carbon and nickel upon the stacking fault energy, *Met. Sci. J.*, **1**, No. 1: 123–127 (1967);
https://doi.org/10.1179/msc.1967.1.1.123
81. P.Yu. Volosevich, V.N. Gridnev, and Yu.N. Petrov, Carbon effect on stacking fault energy of austenite in manganese steels, *Fiz. Met. Metalloved.*, **40**, No. 3: 554–559 (1972) (in Russian).
82. V. Gavriljuk, Yu. Petrov, and B. Shanina, Effect of nitrogen on the electron structure and stacking fault energy in austenitic steels, *Scripta Mater.*, **55**: 537–540 (2006);
https://doi.org/10.1016/j.scriptamat.2006.05.025
83. V.G. Gavriljuk, A.I. Tyshchenko, V.V. Bliznuk, I.L. Yakovleva, S. Riedner, and H. Berns, Cold work hardening of high-strength austenitic steels, *Steel Res. Intern.*, **79**, No. 6: 413–422 (2008);
https://doi.org/10.1002/srin.200806147
84. H. Berns, V.G. Gavriljuk, and S. Riedner, *High Interstitial Stainless Austenitic Steels* (Heidelberg–New York–Dordrecht–London: Springer: 2013);
https://doi.org/10.1007/978-3-642-33701-7
85. V. Gerold and H.P. Karnthaler, On the origin of planar slip in f.c.c. alloys, *Acta Metall.*, **37**, No. 8: 2177–2183 (1989);
https://doi.org/10.1016/0001-6160(89)90143-0
86. J.M. Cowley, X-ray measurement of order in single crystals of Cu_3Au, *J. Appl. Phys.*, **21**, No. 1: 24–30 (1950);
https://doi.org/10.1063/1.1699415
87. H. Warlimont, *Order–Disorder Transformations in Alloys* (Berlin–Heidelberg–

New York: Springer: 1974);
https://doi.org/10.1007/978-3-642-80840-1
88. V.I. Iveronova and A.A. Katsnelson, *Short-Range Order in Solid Solutions*, (Moskva: Nauka: 1977) (in Russian).
89. H.D. Solomon and L.M. Levinson, Mössbauer effect study of '475 °C embrittlement' of duplex and ferritic stainless steels, *Acta Metall.*, **26**, No. 3: 429–442 (1978);
https://doi.org/10.1016/0001-6160(78)90169-4
90. K.A. Kozlov, V.A. Shabashov, A.E. Zamatovskii, V.V. Sagaradze, and K.A. Lyashkov, Atomic ordering in a low-concentrated Fe–Cr alloy upon severe plastic deformation, *Phys. Met. Metallogr.*, **119**, No. 11: 1093–1100 (2018);
https://doi.org/10.1134/S0031918X18110121
91. G.G. Amigood and V.S. Litvinov, Short-range order and stability of austenite in iron–manganese alloys of Fe–20Mn type, *Fiz. Met. Metalloved.*, **56**, No. 6: 1132–1137 (1983) (in Russian).
92. V.N. Bugayev, V.G. Gavriljuk, V.M. Nadutov, and V.A. Tatarenko, Interaction and atomic distribution in fcc alloy FeMnC, *Dokl. Akad. Nauk SSSR*, **288**, No. 2: 362–365 (1986) (in Russian).
93. D.N. Movchan, V.N. Shyvanyuk, B.D. Shanina, and V.G. Gavriljuk, Atomic interactions and hydrogen-induced γ phase in fcc iron–nickel alloys, *Phys. Stat. Sol. A*, **207**, No. 8: 1796–1801 (2010);
https://doi.org/10.1002/pssa.200925548
94. G. Hongxia, Ch. Hua, L. Fan, and Q. Zhenpin, Shape-controlled synthesis of $FeNi_3$ nanoparticles by ambient chemical reduction and their magnetic properties, *J. Mater. Res.*, **27**, No. 11: 1522–1530 (2012);
https://doi.org/10.1557/jmr.2012.67
95. N.Y. Pandya, A.D. Mevada, and P.N. Gajjar, Lattice dynamical and thermodynamic properties of $FeNi_3$, FeNi and Fe_3Ni invar materials, *Comp. Mater. Sci.*, **123**: 287–295 (2016);
https://doi.org/10.1016/j.commatsci.2016.07.001
96. F.A. Garner and J.M. McCarthy, Spinodal-like decomposition of Fe–Ni and Fe–Ni–Cr "invar" alloys during neutron or ion irradiation, *Physical Metallurgy of Controlled Expansion Invar-Type Alloys* (Eds. K.C. Russel and D.F. Smith) (Warendale, PA: TMS-AIME: 1990), pp. 187–206.
97. F. Rotman, D. Gilbon, and O. Dimitro, Periodic decomposition of electron-irradiated pure austenitic Fe–Cr–Ni alloys, *Physical Metallurgy of Controlled Expansion Invar-Type Alloys* (Eds. K.C. Russel and D.F. Smith) (Warendale, PA: TMS-AIME: 1990), pp. 145–158.
98. A. Wiedenmann, W. Wagner, and H. Wollenberger, Thermal decomposition of Fe–34 at.% Ni between 625 °C and 725 °C, *Scripta Metall.*, **23**, No. 4: 603–605 (1989);
https://doi.org/10.1016/0036-9748(89)90459-6
99. B.D. Shanina, V.G. Gavriljuk, A.A. Konchits, S.P. Kolesnik, and A.V. Tarasenko, Exchange interaction between electron subsystems in iron-based fcc alloy doped by nitrogen or carbon, *Phys. Stat. Sol. A*, **149**: 711–722 (1995);
https://doi.org/10.1002/pssa.2211490222
100. B.D. Shanina, V.G. Gavriljuk, A.A. Konchits, and S.P. Kolesnik, The influence of substitutional atoms upon the electron structure of the iron-based transition metal alloys, *J. Phys.: Cond. Mat.*, **10**, No. 8: 1825–1838 (1998);
https://doi.org/10.1088/0953-8984/10/8/015
101. V.G. Gavriljuk and H. Berns, *High Nitrogen Steels* (Berlin: Springer: 1999).
102. V.G. Gavriljuk, B.D. Shanina, and H. Berns, On the correlation between electron

structure and short-range atomic order in iron-based alloys, *Acta Mater.*, **48**: 3879–3893 (2000);
https://doi.org/10.1016/S1359-6454(00)00192-0
103. A. Abragam and B. Blreaney, *Electron Paramagnetic Resonance of Transition Ions* (Oxford: Clarendon Press: 1970).
104. B.D. Shanina, A.I. Tyshchenko, I.N. Glavatskyy, V.V. Runov, Yu.N. Petrov, H. Berns, and V.G. Gavriljuk, Chemical nano-scale homogeneity of austenitic CrMnCN steels in relation to electronic and magnetic properties, *J. Mat. Sci.*, **46**, No. 24: 7725–36 (2011);
https://doi.org/10.1007/s10853-011-5752-9
105. S.R. Chen and D. Tang, Effect of interstitial atom concentration on lattice parameters of martensite and retained austenite in iron–carbon–nitrogen alloys, *Mater. Sci. Forum*, **56–58**: 201–206 (1990);
https://doi.org/10.4028/www.scientific.net/MSF.56-58.201
106. K. Takita and K. Sakamoto, Low temperature internal friction peak and hydrogen cold-work peak in deformed α-iron, *Scr. Metall.*, **10**, No. 5: 399–403 (1976);
https://doi.org/10.1016/0036-9748(76)90160-5
107. A.H. Cottrell and B.F. Bilby, Dislocation theory of yielding and strain ageing of iron, *Proc. Phys. Soc. A*, **6**, No. 1: 49–62 (1949);
https://doi.org/10.1088/0370-1298/62/1/308
108. Y. Yagodzinskyy, M. Ivanchenko, and H. Ндnninen, Hydrogen-dislocation interaction in austenitic stainless steel studied with mechanical loss spectroscopy, *Solid State Phenom.*, **184**: 227–232 (2012);
https://doi.org/10.4028/www.scientific.net/ssp.184.227
109. M.R. Louthan, J.A. Donovan, and G.R. Gaskey, Hydrogen diffusion and trapping in nickel, *Acta Metall.*, **23**, No. 6: 745–749 (1975);
https://doi.org/10.1016/0001-6160(75)90057-7
110. S.M. Teus, Hydrogen mobility and its interaction with dislocations in nickel-based Inconel 718 alloy, *Metallofiz. Noveishie Tecnol.*, **39**, No. 5: 593–606 (2017);
https://doi.org/10.15407/mfint.39.05.0593
111. S.M. Teus, D.G. Savvakin, O.M. Ivasishin, and V.G. Gavriljuk, Hydrogen migration and hydrogen–dislocation interaction in austenitic steels and titanium alloy in relation to hydrogen embrittlement, *Int. J. Hydrogen Energy*, **42**, No. 4: 2424–2433 (2018);
https://doi.org/10.1016/j.ijhydene.2016.09.212
112. D.E. Jiang and E.A. Carter, Diffusion of interstitial hydrogen into and through bcc Fe from first principles, *Phys. Rev. B*, **70**, No. 6: 064102 (2004);
https://doi.org/10.1103/PhysRevB.70.064102
113. M. Nagano, Y. Hayashi, N. Ohtani, M. Isshik, and K. Igaki, Hydrogen diffusivity in high purity alpha iron, *Scr. Metall.*, **16**, No. 8: 973–976 (1982);
https://doi.org/10.1016/0036-9748(82)90136-3
114. S. Fukuyama, D. Sun, L. Zhang, M. Wen, and K. Yokogawa, Effect of temperature on hydrogen environment embrittlement of type 316 series austenitic stainless steels at low temperatures, *J. Jpn. Inst. Met. Mater.*, **67**, No. 9: 456–459 (2003);
https://doi.org/10.2320/jinstmet1952.67.9_456
115. V.G. Gavriljuk, S.P. Efimenko, Ye.E. Smuk, S.Yu. Smuk, B.D. Shanina, N.P. Baran, and V.M. Maksimenko, Electron-spin-resonance study of electron properties in nitrogen and carbon austenite, *Phys. Rev. B*, **48**, No. 5: 3224–3231 (1993);
https://doi.org/10.1103/PhysRevB.48.3224
116. U. Zwicker and H. Schleicher, Titanium alloys deformability improvement technique during hot pressure shaping, *USA Patent No. 2892742, Grade 148-11.5* (1959).

117. B.A. Kolachev, V.K. Nosov, V.A. Lyvanov, G.I. Shypunov, and A.D. Chuchuryukin, Hydrogen effect on technological plasticity of Ti+9% Al alloy, *Izv. Vuzov: Non-Ferrous Metallurgy*, No. 4: 137–142 (1972) (in Russian).
118. B.A. Kolachev, S.A. Vigdorchik, A.V. Malkov, and V.K. Nosov, On a favourable hydrogen effect on technological plasticity of titanium alloy, *Technology of Light Alloys*, No. 7: 32–35 (1974) (in Russian).
119. V.A. Lyvanov, B.A. Kolachev, and V.K. Nosov, On a mechanism of favourable hydrogen effect on technological plasticity of high-aluminum titanium alloys, *Metallurgy and Casting of Light Alloys* (Moskva: Metallurgiya: 1977), pp. 312–320 (in Russian).
120. B.A. Kolachev and V.K. Nosov, Hydrogen plastification and superplasticity of titanium alloys, *Fiz. Met. Metalloved.*, **57**, No. 2: 288–297 (1984) (in Russian).
121. D. Eliezer, N. Eliaz, O. Senkov, and F. Froes, Positive effects of hydrogen in metals, *Mat. Sci. Eng. A*, **280**, No. 1: 220–224 (2000); https://doi.org/10.1016/s0921-5093(99)00670-x
122. F.H. Froes, O.N. Senkov, and J.I. Qasi, Beneficial effects of hydrogen as a temporary alloying element in titanium alloys: An overview, *Int. Symp. Processing and Fabrication of Advanced Materials XI* (Eds. T.S. Srivatsan and R.A. Varin) (Materials Park, OH: ASM International: 2003), pp. 295–305.
123. F.H. Froes, O.N. Senkov, and J.I. Qasi, Hydrogen as a temporary alloying element in titanium alloys: Thermohydrogen processing, *Int. Mater. Rev.*, **49**, Nos. 3–4: 227–245 (2004); https://doi.org/10.1179/095066004225010550
124. B.A. Kolachev, Reversible hydrogen alloying of titanium alloys, *Met. Sci. Heat Treat.*, **35**, 586–591 (1993); https://doi.org/10.1007/BF00778671
125. V.K. Nosov, M. Kolerov, S.A. Mamonov, A.V. Ovchinnikov, and A.A. Krastilevskii, Hydrogen effect on deformability of titanium alloys VT22 and VT22I at ambient temperature, *Metally*, No. 6: 95–99 (1995) (in Russian).
126. V.K. Nosov, A.V. Ovchinnikov, and Y.Y. Shchugorev, Applications of hydrogen plasticizing of titanium alloys, *Metal Sci. Heat. Treat.*, **50**: 378–382 (2008); https://doi.org/10.1007/s11041-008-9059-7
127. Y. Murakami, T. Kanezaki, and Y. Mine, Hydrogen effect against hydrogen embrittlement, *Metall. Mater. Trans A*, **41**, No. 10: 2548–2562 (2010); https://doi.org/10.1007/s11661-010-0275-6
128. R. Kirchheim, Solid solution softening and hardening by mobile solute atoms with special focus on hydrogen, *Scr. Mater.*, **67**, No. 9: 767–770 (2012); https://doi.org/10.1016/j.scriptamat.2012.07.022
129. A. Zielinski, G. Hauptmann, U. Holzwarth, and H. Kronmüller, Internal friction in cold worked and hydrogen charged nickel single crystals, *Z. Metallkd.*, **87**, No. 2: 104–110 (1996); https://doi.org/10.1515/ijmr-1996-870207
130. A. Seeger, The temperature dependence of the critical shear stress and of work-hardening of metal crystals, *Phil. Mag.*, **45**, No. 336: 771–773 (1954); https://doi.org/10.1080/14786440708520489
131. A. Seeger, The generation of lattice defects by moving dislocations, and its application to the temperature dependence of the flow stress of f.c.c. crystals, *Phil. Mag.*, **46**, No. 382: 1194–1217 (1955); https://doi.org/10.1080/14786441108520632
132. B. Obst and A. Nyilas, Experimental evidence on the dislocation mechanism of serrated yielding in f.c.c. metals and alloys at low temperatures, *Mat. Sci. Eng.*

A, **137**: 141–150 (1991));
https://doi.org/10.1016/0921-5093(91)90328-K
133. A. Nyilas, B. Obst, and H. Nakajima, Tensile properties, fracture and crack growth of a nitrogen strengthened new stainless steel (Fe–25Cr–15Ni–0.35N) for cryogenic use, *High Nitrogen Steels* (Eds. V.G. Gavriljuk and V.M. Nadutov) (Kiev: Institute for Metal Physics: 1993), pp. 339–344.
134. V.G. Gavriljuk, A.L. Sozinov, K. Foct, Yu.N. Petrov, and Yu.A. Polushkin, Effect of nitrogen on the temperature dependence of the yield strength of austenitic steels, *Acta Mater.*, **46**, No. 4: 1157–1163 (1998);
https://doi.org/10.1016/S1359-6454(97)00322-4
135. B. Obst, Basic aspects of tensile properties, *Handbook of Applied Superconductivity* (Ed. B. Seeger) (Bristol-Philadelphia: Institute of Physics Publishing: 1998), vol. **2**, F1.1, pp. 969–993.
136. V.G. Gavriljuk, V.M. Shyvaniuk, and S.M. Teus, On the nature of positive hydrogen and nitrogen effects on fatigue of austenitic steels, *Metallofiz. Noveishie Tekhnol.*, **44**, No. 11: 1395–1405 (2022);
https://doi.org/10.15407/mfint.44.11.1395
137. H. Margolin, J. Mahajan, and Y. Saleh, Grain boundaries, stress gradients and fatigue crack initiation, *Scr. Metall.*, **10**, No. 12: 1115–1118 (1976);
https://doi.org/10.1016/0036-9748(76)90036-3
138. J.E. Epperson, P. Fürnrohr, and C. Ortiz, The short-range-order structure of α-phase Cu–Al alloys. *Acta Cryst. A*, **34**: 667–681 (1978);
https://doi.org/10.1107/s0567739478001424
139. R.L. Tobler and R.P. Reed, Interstitial carbon and nitrogen effects on the cryogenic fatigue crack growth of AISI 304 type stainless steels, *J. Testing Evaluation*, **12**: 364–370 (1984);
https://doi.org/10.1520/JTE10741J
140. R. Taillard and J. Foct, Mechanisms of the action of nitrogen interstitials upon low cycle fatigue behaviour of 316 stainless steels, *High Nitrogen Steels* (Eds. J. Foct and A. Hendry) (London: The Institute of Metal: 1989), pp. 387–391.
141. Y. Ogawa, H. Hosoi, K. Tsuzaki, T. Redarce, O. Takakuwa, and H. Matsunaga, Hydrogen, as an alloying element, enables a greater strength-ductility balance in an Fe–Cr–Ni-based, stable austenitic stainless steel, *Acta Mater.*, **199**: 181–192 (2020);
https://doi.org/10.1016/j.actamat.2020.08.024
142. V.N. Shyvanyuk, J. Foct, and V.G. Gavriljuk, Hydrogen-enhanced microplasticity of austenitic steels studied by means of internal friction, *Mat. Sci. Eng. A*, **300**, Nos. 1–2: 284–290 (2001);
https://doi.org/10.1016/S0921-5093(00)01442-8
143. V.G. Gavriljuk, B.D. Shanina, V.N. Shyvanyuk, and S.M. Teus, Hydrogen embrittlement of austenitic steels: electron approach, *Corros. Rev.*, **31**, No. 2: 33–50 (2013);
https://doi.org/10.1515/corrrev-2013-0024
144. V.G. Gavriljuk, S.M. Teus, B.D. Shanina, and A.A. Konchits, On the nature of similarity in embrittlement of metals by hydrogen and surfactants, *Material Sci. & Eng. Int. J.*, **1**, No. 3: 70–79 (2017);
https://doi.org/10.15406/mseij.2017.01.00013
145. S.M. Teus, D.G. Savvakin, O.M. Ivasishin, and V.G. Gavriljuk, Hydrogen migration and hydrogen-dislocation interaction in austenitic steels and titanium alloy in relation to hydrogen embrittlement, *Int. J. Hydrogen Energy*, **42**, No. 4: 2424–2433 (2016);
https://doi.org/10.1016/j.ijhydene.2016.09.212

Received 20.02.2024
Final version 02.08.2024

В.Г. Гаврилюк, В.М. Шиванюк, С.М. Теус
Інститут металофізики ім. Г.В. Курдюмова НАН України,
бульв. Академіка Вернадського, 36, 03142 Київ, Україна

ЕЛЕКТРОННА КОНЦЕПЦІЯ ВОДНЕВОГО ОКРИХЧЕННЯ ТА ПІДВИЩЕНОЇ ПЛАСТИЧНОСТІ МЕТАЛІВ

На основі теоретичних і експериментальних досліджень впливу Гідрогену на електронну структуру заліза, нікелю та титану запропоновано електронну концепцію водневого окрихчення та поліпшеної Гідрогеном пластичності конструкційних металевих матеріалів. Запропонована концепція передбачає перерозподіл валентних електронів по енергетичних рівнях зі збільшенням густини електронних станів на рівні Фермі, що зумовлює пом'якшення кристалічної ґратки та зменшення питомої енергії дислокацій із відповідним підвищенням їхньої рухливості. Природні властивості металевих твердих розчинів, а саме близький атомний порядок у його двох проявах — близьких впорядкуванні та розпаді, аналізуються як передумова локалізації пластичної деформації. Гідроген лише посилює ефект локалізованої пластичності завдяки різній його розчинності в субмікрооб'ємах упорядкованого твердого розчину, що призводить до псевдокрихкого руйнування. Проаналізовано роль індукованих Гідрогеном надлишкових вакансій у локалізації пластичної деформації та водневому зерномежовому руйнуванні чистих металів. Методами температуро- та деформаційно-залежного внутрішнього тертя досліджено ентальпії дифузії Гідрогену та зв'язку атомів Гідрогену з дислокаціями, продемонстровано контролювальний вплив їх на залежність водневого окрихчення від температури та швидкості деформації. Наприкінці запропоновано фізичне обґрунтування для використання водню як тимчасового легувального елементу в технології температурно-деформаційного оброблення титанових сплавів і поліпшення втомної міцності та пластичності аустенітних сталей.

Ключові слова: водень, залізо, нікель, титан, електронна структура, окрихчення, пластичність.